
PERGAMON

Journal of Quantitative Spectroscopy & Radiative Transfer 75 (2002) 129–175

Journal of Quantitative Spectroscopy & Radiative Transfer

www.elsevier.com/locate/jqsrt

Simultaneous derivation of intensities and weighting functions in a general pseudo-spherical discrete ordinate radiative transfer treatment

R.J.D. Spurr *

Harvard-Smithsonian Center for Astrophysics, 60 Garden Street, Cambridge, MA 02138, USA

Received 21 November 2000; accepted 14 March 2001

Abstract

The retrieval of atmospheric constituents from measurements of backscattered light requires a radiative transfer forward model that can simulate both intensities and weighting functions (partial derivatives of intensity with respect to atmospheric parameters being retrieved). The radiative transfer equation is solved in a multi-layer multiply-scattering atmosphere using the discrete ordinate method. In an earlier paper dealing with the upwelling top-of-the-atmosphere radiation field, it was shown that a full internal perturbation analysis of the plane-parallel discrete ordinate solution leads in a natural way to the simultaneous generation of analytically-derived weighting functions with respect to a wide range of atmospheric variables. In the present paper, a more direct approach is used to evaluate explicitly all partial derivatives of the intensity field. A generalization of the post-processing function is developed for the derivation of weighting functions at arbitrary optical depth and stream angles for both upwelling and downwelling directions. Further, a complete treatment is given for the pseudo-spherical approximation of the direct beam attenuation; this is an important extension to the range of viewing geometries encountered in practical radiative transfer applications. The numerical model LIDORT developed for this work is able to generate intensities and weighting functions for a wide range of retrieval scenarios, in addition to the passive remote sensing application from space. We present a number of examples in an atmosphere with O_3 absorption in the UV, for satellite (upwelling radiation) and ground-based (downwelling radiation) applications. In particular, we examine the effect of various pseudo-spherical parameterizations on backscatter intensities and weighting functions with respect to O_3 volume mixing ratio. In addition, the use of layer-integrated multiple scatter output from the model is shown to be important for satellite instruments with wide-angle off-nadir viewing geometries. Published by Elsevier Science Ltd.

Keywords: Radiative transfer; Discrete ordinates; Linearization; Pseudo-spherical

* Tel.: +1-617-496-7819; fax: +1-617-495-7389.
E-mail address: rspurr@cfa-harvard.edu (R.J.D. Spurr).

0022-4073/02/$ - see front matter. Published by Elsevier Science Ltd.
PII: S0022-4073(01)00245-X

1. Introduction

1.1. Background and rationale

Measuring the Earth's atmosphere is an essential requirement for the understanding of physical and chemical processes that determine radiative balance. This is particularly important in the light of possible climate change induced by man's activities on this planet. A key ingredient in atmospheric monitoring is the retrieval of surface properties and atmospheric constituent distributions from measurements of earthshine radiation. This applies not only to in-situ measurements from ground-based instruments and local measurements from aircraft and balloons, but also to the global coverage provided by passive remote sensing satellite instruments.

Given a state vector $\mathbf{X}$ of atmospheric constituents, we may generate a vector $\mathbf{Y}$ of synthetic radiance measurements at different wavelengths or geometries through the symbolic relation $\mathbf{Y}=F(\mathbf{X})$, where F is the *forward model* describing the attenuation and scattering of light in the atmosphere. Retrieval involves the solution of the inverse problem $\mathbf{X} = F^{-1}(\mathbf{Y})$. This is commonly done by iteration based on a series of linear inversion steps. The *linearization* of the forward model is given by $\mathbf{Y} - \mathbf{Y}_n = \mathbf{K}(\mathbf{X} - \mathbf{X}_n)$, where the matrix $\mathbf{K}$ is the set of *weighting functions* (intensity partial derivatives with respect to atmospheric parameters to be retrieved), and $\mathbf{Y}_n = F(\mathbf{X}_n)$ is the synthetic measurement vector corresponding to state vector estimate $\mathbf{X}_n$ at iteration step n. The inversion is carried out using cost-function minimization techniques such as non-linear least squares fitting [1], the widely-used optimal estimation method [2], or other methods such as Phillips–Tikhonov regularization [3]. All such iterative fitting methods require a radiative transfer model that will simultaneously generate both intensities and weighting functions.

The main purpose behind this paper and the previous work (Spurr, Kurosu and Chance [4], hereafter denoted by SKC) is to develop a general radiative transfer tool LIDORT with the capability to generate simultaneous and accurate intensity and weighting function fields. The discrete ordinate method is used to solve the radiative transfer equation (RTE). In SKC, the intensity model and its weighting function linearization were developed for upwelling radiation fields at top-of-atmosphere (TOA) in a plane-parallel geometry. The aim of the present paper is to extend and generalize the LIDORT model, and to develop new tools for dealing with a wider range of atmospheric scenarios.

In the discrete ordinate formalism [5,6], the intensity calculation depends only on knowledge of optical depths, single scattering albedos and phase function moments. Preparation of these quantities depends on the application and is carried out beforehand. The discrete ordinate method is a *generic* scattering formalism; it is not necessary to know the composition and detailed physics of the medium in question in order to solve the radiative transfer problem. The DISORT package [6] was developed with this philosophy in mind, and it is the most flexible and widely-used plane-parallel radiative transfer tool available to the atmospheric community. We adopt the same strategy for LIDORT, that is, to maintain the generic nature of the scattering formalism, but to develop extensions to generate weighting functions as well as intensities, for both plane-parallel and pseudo-spherical geometries.

In this work, the evaluation of weighting functions is based on an explicit analytic determination of partial derivatives of all components of the discrete ordinate solution for intensity. In line with the above remark on linearizing the forward model, we use the term *linearization analysis* to indicate the process of obtaining the set of partial derivatives that constitute the matrix of weighting functions. (A different emphasis was used in SKC, where weighting functions were determined through

a complete first-order perturbation analysis of the discrete ordinate solution.) All weighting functions are determined analytically to the same accuracy as the intensity field. LIDORT can compute weighting functions with respect to a wide range of atmospheric variables; as with DISORT, the tool is not application-specific. In addition to the above-mentioned optical properties required as input to the intensity calculation, LIDORT requires as input for the weighting function calculations the derivatives of layer single scattering albedos and extinction coefficients with respect to the set of atmospheric parameters for which weighting functions are required.

For an intensity-only RT model without the linearization capability, weighting functions must be estimated using finite-difference methods; in a multi-parameter retrieval, this involves many separate calls to the model. With LIDORT, a single call will generate the set of intensities and weighting functions at one wavelength required for an iteration step in a typical multi-parameter atmospheric retrieval; this represents a very substantial saving of computer effort. Furthermore, the analytically accurate derivation of LIDORT weighting functions avoids concerns over the accuracy of finite-difference estimates based on *ad hoc* choices of the external perturbations. We note that at the present time, to our knowledge, only the GOMETRAN RT model [7,8] has the capability to generate simultaneous fields of intensity and analytically accurate weighting functions.

Weighting functions with respect to ozone volume mixing ratio are important for the retrieval of ozone profiles from nadir-viewing remote sensing instruments measuring in the UV and visible. A full multiple-scatter RT treatment is a necessary requirement in this part of the spectrum. This retrieval problem has been discussed in the context of the GOME [9] instrument in a number of studies [10–13]. In the present work, we will give examples of LIDORT output for a terrestrial atmosphere scenario relevant to the ozone profile retrieval context, not only for GOME but also for future instruments such as SCIAMACHY [14], GOME-2 [15] and OMI [16]. A fast 4-stream version of LIDORT has recently been developed for use in near-real-time ozone profile retrieval algorithms for these instruments [17].

Many atmospheric RT problems can be treated using the assumption of a plane-parallel medium. However, this assumption breaks down for solar zenith angles and/or line-of-sight viewing angles approaching 90°, and it then becomes necessary to make some allowance for the sphericity of the atmosphere. This is particularly important for polar-orbiting satellite instruments such as GOME, for which large solar zenith angles are frequently encountered. In a stratified spherical-shell medium, the intensity field changes with angular variables (solar and line of sight zenith angles, relative azimuth angle between planes containing the line of sight and solar directions) in addition to the zenith variation with optical depth.

The *pseudo-spherical* assumption ignores these angular derivatives; only the variation of intensity with the vertical coordinate is present in the RTE. The attenuation of the direct beam to the point of scatter is treated for a curved spherical-shell atmosphere (see Fig. 1); apart from the transmittance calculation for single scatter, all higher-order scattering events are treated as locally plane-parallel. In a pseudo-spherical RT model, scattering takes place along the local vertical AC in Fig. 1. It has been shown [18,19] that the pseudo-spherical approximation provides a useful and sufficiently accurate RT intensity simulation for solar zenith angles up to 90°, provided that the line-of-sight is reasonably close to the nadir. A pseudo-spherical model is adequate for simulating backscatter intensities and weighting functions for the GOME and SCIAMACHY instruments in their normal nadir scanning modes (where the off-nadir scan angle does not exceed 31° at the satellite). The great advantage of this approach is that it utilizes the power, speed and flexibility of the plane-parallel

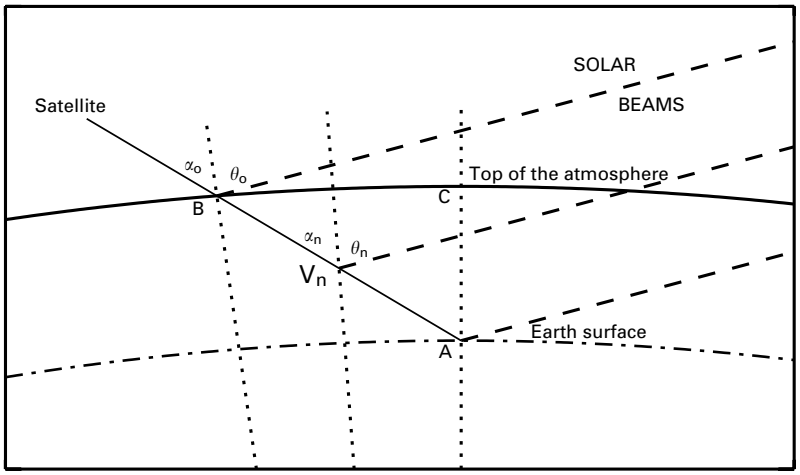

Fig. 1. Satellite viewing geometry in a curved spherical-shell atmosphere.

discrete scattering formalism, and avoids the greatly more complex and computationally intensive full-spherical RT treatment.

It is possible to extend such a model to deal with wide off-nadir satellite viewing conditions (angle α_0 in Fig. 1 up to 70°); such geometry will be encountered routinely with the GOME-2 and OMI instruments. We consider scattering events along line AB instead of the vertical AC assumed for the regular pseudo-spherical computation. The basic idea behind the extension for wide-angle nadir satellite geometry is to make precise calculations of the single scatter contributions along AB (with both solar and line-of-sight transmittances for a curved atmosphere), but to approximate the *multiple-scatter* contributions using regular pseudo-spherical output for points along AB. In a detailed study for the TOMS project [19], it was shown that the major source of error in the regular pseudo-spherical model arises from an incorrect computation of the single scatter terms. We shall call this extension the *enhanced pseudo-spherical model*. Given the LIDORT capability to generate both intensities and weighting functions, it is then possible to use the enhanced model in profile retrieval algorithms in wide-angle viewing scenarios.

The accuracy of the pseudo-spherical approximation depends on the parameterization used to describe the direct beam attenuation. For most cases, the *average secant* parameterization is sufficient: in a multi-layer atmosphere, slant path transmittances are taken to be exact at layer boundaries, with a simple exponential in optical thickness to approximate the attenuation across layers. The main LIDORT development is based on this assumption. However, we will examine more accurate parameterizations of direct beam transmittance in situations with optically thick layers. In any case, the *particular* solution to the discrete ordinate RTE must be modified to deal with the solar beam attenuation in a curved atmosphere (the *homogeneous* solutions are unchanged). In this work, we will examine two different approaches to the particular integral solution for the direct solar beam: the classical substitution method first used by Chandrasekhar [5] and standard in DISORT, and secondly, the more recent Green's function technique developed by Siewert and co-workers ([20] and references therein). Particular solutions for atmospheric thermal emission source terms will not be considered here; a derivation of TOA intensity and weighting functions for thermal emission

sources in a plane-parallel atmosphere was given in SKC [4]. As in SKC, we shall consider only the solution to the scalar RTE; polarization will not be considered.

The generalization to arbitrary optical depth and stream angle involves the further development and extension of the *post-processing function*, in which the discrete ordinate solution is used to interpolate both the intensity and the weighting functions to arbitrary polar viewing angles. The approach adopted here is the standard source function integration technique [5,21]. Output options for standard angle-integrated quantities (azimuthally-independent fluxes and mean intensities and associated weighting functions) have been incorporated in the model. The delta-M scaling transformation [22] is also a standard feature in the new version. LIDORT will also generate layer-integrated multiple scatter source terms and their weighting functions; as noted above, this output is an essential part of the enhanced pseudo-spherical model for RT simulation in wide-angle off-nadir satellite viewing geometries.

1.2. Organization of the paper

Section 2 is a brief recapitulation of the discrete ordinate solution to the RTE in a multi-layer atmosphere with a pseudo-spherical parameterization of the beam source attenuation. We summarize solutions for the homogeneous RTE equation, the boundary-value determination of integration constants from the boundary conditions, and the post-processing function. Determination of the particular solutions is deferred to the following section. In Section 3.1, we introduce three parameterizations for the attenuation of the direct beam in a curved atmosphere; these are the *average secant*, the *exponential-sine* and the *exponential-polynomial* parameterizations. In Sections 3.2 and 3.3 we determine, respectively, the classical and Green's function solutions for the particular integral using the average secant parameterization. In addition, in Section 3.3, the Green's function technique is used to derive more accurate solutions based on the other parameterizations of the direct beam attenuation.

In Section 4, we look at the linearization analysis. For a set of atmospheric parameters in a given layer for which we desire weighting functions, we require the derivatives of the extinction coefficient and single scattering albedo in that layer with respect to these parameters; these derivatives then determine the rules for the linearization analysis (Section 4.1). Once the latter are specified, the evaluation of intensity partial derivatives follows the same sequence of steps required for the complete intensity solution. In Sections 4.2 and 4.3 we apply the linearization analysis to the homogeneous and particular solutions, followed by the linearized boundary value problem (Section 4.4) and the post-processing function for generalized weighting function output in Section 4.5. The particular solution linearization in this section is restricted to the average secant parameterization.

Section 5 gives a brief description of the LIDORT software package based on the theory of the preceding sections. We give some comparisons with DISORT and SDISORT [23] output, and discuss the issue of weighting function validation. Section 6 contains some examples. The main emphasis here is on the satellite application for the retrieval of ozone profiles from nadir UV backscatter measurements. We concentrate on ozone absorption in the Hartley–Huggins bands (290–335 nm), and consider weighting functions with respect to ozone volume mixing ratio. Intensities and weighting functions are compared in the pseudo-spherical and plane-parallel approximations. Examples of output appropriate for ground-based instruments are also presented. In Section 6.3, we illustrate the

use of the enhanced pseudo-spherical LIDORT model to improve intensity and weighting function simulations for the GOME, GOME-2, SCIAMACHY and OMI instruments at wide-angle viewing geometries.

2. Discrete ordinate theory: pseudo-spherical source function

2.1. The radiative transfer equation (RTE)

We consider the solution of the RTE in the pseudo-spherical approximation. Scattering will be non-conservative. We summarize the homogeneous solutions to the discrete ordinate equations, the boundary value problem and the post-processing function. Derivations of the particular solutions are deferred until Section 3; however, the role played by the particular solution will be outlined here. Although the theory summarized here may be found in various places (see for example [21] and references therein), it is important to have each stage of the discrete ordinate intensity solution clearly laid out in order to facilitate the linearization analysis in Section 4.

The RTE for the *diffuse* intensity $I(\tau,\mu,\phi)$ is:

$$\mu\frac{\mathrm{d}I(\tau,\mu,\phi)}{\mathrm{d}\tau} = I(\tau,\mu,\phi) - \frac{\omega(\tau)}{4\pi}\int_0^{2\pi}\mathrm{d}\phi'\int_{-1}^{1}\mathrm{d}\mu' P(\tau,\mu,\phi;\mu',\phi')I(\tau,\mu',\phi') - S_{\odot}(\tau,\mu,\phi). \tag{1}$$

Here, τ is the optical depth of the medium, μ is the absolute value of the cosine of the polar angle cosine (measured with respect to the zenith), and ϕ is the azimuth angle measured with respect to a suitable axis perpendicular to the zenith. $\omega(\tau)$ is the single scattering albedo, and $P(\tau,\mu,\phi;\mu',\phi')$ the phase function. For a parallel beam of net incident flux $\mu_0\pi F_{\odot}$ and direction $\{-\mu_0,\phi_0\}$ at the top of the atmosphere ($\tau=0$), the single scattering source term is:

$$S_{\odot}(\tau,\mu,\phi) = \frac{F_{\odot}}{4}\omega(\tau)P(\tau,\mu,\phi;-\mu_0,\phi_0)\mathrm{e}^{-\tau_{\mathrm{spher}}(\tau)}. \tag{2}$$

The solar beam transmittance is expressed in terms of a slant path optical depth $\tau_{\mathrm{spher}}(\tau)$ which is a function of τ. For now, we will not deal with this term explicitly, referring to the next section for particular integral derivations using explicit parameterizations of this transmittance. We note that the *total* intensity is actually the sum of the diffuse field $I(\tau,\mu,\phi)$ in (1) and an unscattered sunlight term $I_{\mathrm{sun}}(\tau,\mu,\phi)$ given by:

$$I_{\mathrm{sun}}(\tau,\mu,\phi) = \pi F_{\odot}\mathrm{e}^{-\tau_{\mathrm{spher}}(\tau)}\delta(\mu-\mu_0)\delta(\phi-\phi_0). \tag{3}$$

We assume the atmosphere is divided into a number of homogeneous layers, each layer having uniform optical properties. We first consider the solutions for a single layer, with single scattering albedo and phase functions regarded as independent of τ. The intensity is expanded as a Fourier cosine series in the relative azimuth $\phi-\phi_0$:

$$I(\tau,\mu,\phi) = \sum_{m=0}^{2N-1} I^m(\tau,\mu)\cos m(\phi-\phi_0). \tag{4}$$

Using the expansion of the phase function in terms of Legendre polynomials in the cosine of the scatter angle, plus the addition theorem for Legendre functions, the azimuthal dependence of P can also be expressed as a cosine series in relative azimuth. The azimuth separation follows immediately, and we obtain the following for each Fourier component m:

$$\mu \frac{\mathrm{d}I^m(\tau,\mu)}{\mathrm{d}\tau} = I^m(\tau,\mu) - S^m(\tau,\mu), \tag{5}$$

$$S^m(\tau,\mu) = \int_{-1}^{1} \Pi^m(\mu,\mu') I^m(\tau,\mu')\,\mathrm{d}\mu' - \frac{F_\odot}{2}(2-\delta_{m0})\Pi^m(\mu,-\mu_0)\mathrm{e}^{-\tau_{\mathrm{spher}}(\tau)}, \tag{6}$$

where $m = 0, 1, \ldots, 2N-1$, and δ_{m0} is 1 for $m = 0$ and vanishes for $m \neq 0$. The auxiliary quantities Π^m are defined in terms of *normalized* Legendre polynomials $P_l^m(\mu)$ and phase function moment coefficients β_l (the actual Legendre expansion moments are $\beta_l/(2l+1)$) through

$$\Pi^m(\mu,\mu') = \frac{\omega}{2} \sum_{l=m}^{2N-1} \beta_l P_l^m(\mu) P_l^m(\mu'). \tag{7}$$

To obtain discrete ordinate solutions, we replace the multiple-scatter integral in (6) with a summation using two Gauss–Legendre quadratures defined separately in each polar angle half-space. Each quadrature has N points, with abscissae and weights $\{\mu_i, w_i\}$, $i = 1, \ldots, N$ in the positive half-space, and $\{-\mu_i, w_i\}$, $i = 1, \ldots, N$ for the negative half-space. The advantages of the double quadrature scheme have been discussed in the literature (see for example [21]). Eqs. (5) and (6) are then replaced by the discrete ordinate form:

$$\mu_i \frac{\mathrm{d}I^m(\tau,\mu_i)}{\mathrm{d}\tau} = I^m(\tau,\mu_i) - \sum_{j=\pm 1}^{j=\pm N} w_j \Pi^m(\mu_i,\mu_j) I^m(\tau,\mu_j) - Q^m(\mu_i)\mathrm{e}^{-\tau_{\mathrm{spher}}(\tau)}, \tag{8}$$

$$Q^m(\mu_i) = \frac{F_\odot}{2}(2-\delta_{m0})\Pi^m(\mu_i,-\mu_0). \tag{9}$$

2.2. Homogeneous solutions

To get solutions of the homogeneous version of (8), we substitute $I_j \propto X_j \mathrm{e}^{-k\tau}$ for $j = \pm 1, \ldots, \pm N$. By using the sum and difference vectors $\varsigma_j = X_j + X_{-j}$ and $\vartheta_j = X_j - X_{-j}$ for $j = 1, \ldots, N$, (8) can be reduced to an N-rank eigenproblem with eigenvalues k_α^2 and eigenvectors $\boldsymbol{\varsigma}_\alpha$:

$$(\boldsymbol{\Gamma} - k^2 \hat{\mathbf{E}})\boldsymbol{\varsigma} = 0, \quad \text{where } \boldsymbol{\Gamma} = (\boldsymbol{\xi} - \boldsymbol{\eta})(\boldsymbol{\xi} + \boldsymbol{\eta}), \tag{10}$$

$$\zeta_{ij} = (\Pi_{ij}^+ w_j - \delta_{ij})/\mu_i \quad \text{and} \quad \eta_{ij} = \Pi_{ij}^- w_j/\mu_i. \tag{11}$$

Separation constants $\pm k_\alpha$ occur in pairs. In the above equations, $\alpha = 1, \ldots, N$, $\hat{\mathbf{E}}$ is the unit matrix and the elements $\Pi_{ij}^\pm = \Pi^\pm(\mu_i, \pm\mu_j)$ are given by (7) evaluated at quadrature polar angle cosines. The difference vector $\boldsymbol{\vartheta}_\alpha$ satisfies the following auxiliary equation linking it to the eigenvector $\boldsymbol{\varsigma}_\alpha$:

$$k_\alpha \vartheta_{i\alpha} = \sum_{j=1}^{N} (\zeta_{ij} + \eta_{ij})\varsigma_{j\alpha}. \tag{12}$$

Eqs. (10) and (12) are sufficient to determine the solution of the homogeneous equations. The eigenproblem in (10) can be solved reliably using standard numerical routines. We assume that the eigenvectors ς_α have unit length. If we define $2N$-vectors $\mathbf{X}_\alpha^{(P)}$ and $\mathbf{X}_\alpha^{(N)}$ such that

$$X_{j\alpha}^{(P)} = \frac{\varsigma_{j\alpha} + \vartheta_{j\alpha}}{2} \quad \text{and} \quad X_{-j\alpha}^{(P)} = \frac{\varsigma_{j\alpha} - \vartheta_{j\alpha}}{2}, \tag{13}$$

$$X_{j\alpha}^{(N)} = X_{-j\alpha}^{(P)} \quad \text{and} \quad X_{-j\alpha}^{(N)} = X_{j\alpha}^{(P)}, \tag{14}$$

where $j = 1, \ldots, N$, then the complete *homogeneous* solution is

$$I_j(x) = \sum_{\alpha=1}^{N} \{\tilde{L}_\alpha X_{j\alpha}^{(P)} \mathrm{e}^{-k_\alpha \tau} + \tilde{M}_\alpha X_{j\alpha}^{(N)} \mathrm{e}^{+k_\alpha \tau}\}, \tag{15}$$

where $\tilde{L}_\alpha$ and $\tilde{M}_\alpha$ are integration constants.

2.3. The boundary value problem

We assume that a particular solution $G(\tau, \mu_j)$ corresponding to the source term $Q^m(\mu_j)\mathrm{e}^{-\tau_{\mathrm{spher}}(\tau)}$ in (8) has been found. Consider first a single layer p with upper and lower optical depths given by τ_{p-1} and τ_p respectively, and optical thickness $\Delta_p = \tau_p - \tau_{p-1}$. Rather than use the cumulative optical depth τ as the vertical coordinate, we express the homogeneous and particular solutions in terms of the partial layer optical thickness $x = \tau - \tau_{p-1}$. The complete solution for the discrete ordinate components of the intensity field in the layer is:

$$I_{jp}(x) = \sum_{\alpha=1}^{N} \{L_{p\alpha} X_{jp\alpha}^{(P)} \mathrm{e}^{-k_{p\alpha} x} + M_{p\alpha} X_{jp\alpha}^{(N)} \mathrm{e}^{-k_{p\alpha}(\Delta_p - x)}\} + G_p(x, \mu_j). \tag{16}$$

This is valid for upwelling and downwelling streams, $j = \pm 1, \ldots \pm N$. The integration constants $L_{p\alpha}$ and $M_{p\alpha}$ will be determined from the boundary value problem. The definition with x and $\Delta - x$ is equivalent to the scaling transformation suggested by Stamnes and Conklin [24] to express homogeneous transmission factors as negative exponentials; this ensures the stability of the numerical solution.

In a multi-layer atmosphere with K homogeneous layers and $K+1$ layer boundaries, the boundary conditions are:

(BC1) no downward diffuse radiation at the top of atmosphere;
(BC2) continuity of the intensity field at all intermediate levels;
(BC3) a surface reflection condition at the lowest level.

For the reflectance of the lower boundary, we use an expansion of the bi-directional surface reflection function $\rho(\mu, \phi; \mu', \phi')$ in terms of a Fourier series in the cosine of the relative azimuth. The condition for the mth Fourier component of the reflected intensity (diffuse and direct) at the lower boundary is then

$$I^m(\tau_K, +\mu_i) = (1 + \delta_{m0}) \sum_{j=1}^{N} \mu_j w_j I^m(-\mu_j) \rho_m(\mu_i, -\mu_j) + \mu_0 F_\odot \mathrm{e}^{-\tau_{\mathrm{spher}}(\tau_K)} \rho_m(\mu_i, -\mu_0), \tag{17}$$

where $i=1,\ldots,N$, $\tau_{\rm spher}(\tau_K)$ is the slant optical depth of the whole atmosphere (total vertical optical depth τ_K), and ρ_m are the bi-directional Fourier coefficients with polar angles as indicated. As in SKC, we use a normalized form ρ^* of the bi-directional reflection function:

$$\rho_m(\mu_i,-\mu_j)=R\rho_m^*(\mu_i,-\mu_j) \qquad \text{with } R=\frac{1}{4}\int_0^1\int_0^1 \mu\mu'\rho_0(\mu,-\mu')\,\mathrm{d}\mu\,\mathrm{d}\mu', \tag{18}$$

where R is the spherical albedo. For a Lambertian surface, $\rho_0^*(\mu_i,-\mu_j)=1$ and $\rho_m^*(\mu_i,-\mu_j)=0$ for $m>0$, where $i,j=1,\ldots,N$.

We can now write down expressions for the boundary conditions. We introduce the indices p, q, and r to label layers. BC1 is

$$\sum_{\alpha=1}^{N}\{L_{1\alpha}X_{-j1\alpha}^{(P)}+M_{1\alpha}\Theta_{1\alpha}X_{-j1\alpha}^{(N)}\}=-G_{-j1}|_{\tau=0}, \tag{19}$$

where $G_{jp}=G(\tau,\mu_j)$ for τ in layer p. In (19), $j=1,\ldots N$, and $-j$ denotes the downwelling stream directions. On the right-hand side, the particular integral is evaluated at the optical depth indicated. The transmittance factors $\Theta_{p\alpha}$ are defined by

$$\Theta_{p\alpha}=\exp(-k_{p\alpha}\Delta_p), \tag{20}$$

where $\alpha=1,\ldots N$, and $\Delta_p=(\tau_p-\tau_{p-1})$ is the optical thickness of layer p. BC2 is

$$\sum_{\alpha=1}^{N}[\{L_{r\alpha}\Theta_{r\alpha}X_{jr\alpha}^{(P)}+M_{r\alpha}X_{jr\alpha}^{(N)}\}-\{L_{p\alpha}X_{jp\alpha}^{(P)}+M_{p\alpha}\Theta_{p\alpha}X_{jp\alpha}^{(N)}\}]=(G_{jp}-G_{jr})|_{\tau_r}, \tag{21}$$

where $r=p-1$. This is valid for both upwelling and downwelling directions $j=\pm1,\ldots,\pm N$, and for $p=2,\ldots,K$. BC3 at the lower boundary $\tau=\tau_K$ $(p=K)$ is

$$\sum_{\alpha=1}^{N}\{L_{K\alpha}\Theta_{K\alpha}\Phi_{j\alpha}^{(P)}+M_{K\alpha}\Phi_{j\alpha}^{(N)}\}=R\mu_0F_\odot\rho_m^*(\mu_j,-\mu_0)\mathrm{e}^{-\tau_{\rm spher}(\tau_K)}-\Psi_j, \tag{22}$$

where

$$\Phi_{j\alpha}^{(P)}=X_{jK\alpha}^{(P)}-(1+\delta_{m0})R\sum_{i=1}^{N}w_i\mu_i\rho_m^*(\mu_j,-\mu_i)X_{-iK\alpha}^{(P)} \quad \text{and similarly for } \Phi_{j\alpha}^{(N)}, \tag{23a}$$

$$\Psi_j=G_{jK}|_{\tau_K}-(1+\delta_{m0})R\sum_{i=1}^{N}w_i\mu_i\rho_m^*(\mu_j,-\mu_i)G_{-iK}|_{\tau_K}. \tag{23b}$$

The normalized bi-directional reflectance coefficients have been used in BC3, and $\mathrm{e}^{-\tau_{\rm spher}(\tau_K)}$ is the whole atmosphere solar beam transmittance. Eq. (22) is valid for $j=1,\ldots,N$. It is possible to write down a surface boundary to include surface blackbody thermal emission in BC3 [21].

BC1, BC2 and BC3 together constitute a linear algebra system $\mathscr{A}\mathscr{X}=\mathscr{B}$ of order $2NK$. The vector $\mathscr{X}$ consists of the unknown integration constants $L_{p\alpha}$ and $M_{p\alpha}$. Matrix $\mathscr{A}$ has $3N-1$ sub- and super-diagonals; it may be compressed into band-storage form and then inverted using standard

methods (the LAPACK [25] modules DGBTRF for the LU-decomposition and DGBTRS for the back-substitution were used in the numerical model).

2.4. The post-processing function and the complete solution

Finding the intensity for arbitrary direction μ and optical depth τ is known as "post-processing" of the RTE solution. We use the source function integration technique, which relies on the formal integration of (5); it has a clear physical interpretation, and is convenient to use numerically. It is essentially a form of interpolation for the intensity [21]. For a single layer with upper and lower boundary optical depths τ_U and τ_B, the upwelling and downwelling intensities at any intermediate layer optical thickness $x = \tau - \tau_U$ are given by

$$I^+(x,\mu) = I_B^+(\mu)e^{-(\Delta-x)/\mu} + \Lambda^+(x,\mu) \tag{24a}$$

$$I^-(x,\mu) = I_U^-(\mu)e^{-x/\mu} + \Lambda^-(x,\mu), \tag{24b}$$

where $\Delta = \tau_B - \tau_U$ and the *integrated* source terms are

$$\Lambda^+(x,\mu) = e^{x/\mu}\int_x^\Delta J^+(y,\mu)e^{-y/\mu}\frac{dy}{\mu}, \tag{25a}$$

$$\Lambda^-(x,\mu) = e^{-x/\mu}\int_0^x J^-(y,\mu)e^{y/\mu}\frac{dy}{\mu}. \tag{25b}$$

Here $J^\pm(y,\mu)$ is a sum of the multiply-scattered source term intensity at optical thickness y in direction μ and the term due to single scattering of the direct beam into this direction. The first of these terms is evaluated by approximating the multiple-scatter integral by its discrete-ordinate quadrature, using the discrete-ordinate solutions already obtained in (16). Without going into details of the derivation, we can write:

$$\Lambda^\pm(x,\mu) = H^\pm(x,\mu) + D^\pm(x,\mu) + E^\pm(x,\mu), \tag{26}$$

where the three terms represent contributions from the integrated homogeneous solutions, the integrated particular solution and the integrated single scatter term, respectively. The single scatter contribution $E^\pm(x,\mu)$ and the particular solution contribution $D^\pm(x,\mu)$ both depend on the beam attenuation parameterization and the latter depends also on the method used to determine the particular solution. The homogeneous solution term $H^\pm(x,\mu)$ is independent of these aspects. Expressions for $H^\pm(x,\mu)$ may be found in [21] and are noted in Appendix B.1. For now we defer discussion of the single scatter term $E^\pm(x,\mu)$ to the appropriate place in Section 3.1, while the particular solution contributions $D^\pm(x,\mu)$ will be treated later on when we consider the form taken by the particular solution (Sections 3.2, 3.3).

In an inhomogeneous atmosphere, source terms must be integrated on a layer-by-layer basis. Denoting $I_{p-1}^\pm(\mu)$ and $I_p^\pm(\mu)$ for the upwelling and downwelling intensities at the upper and lower boundaries of layer p, respectively, we have from (24a) and (24b):

$$I_{p-1}^+(\mu) = I_p^+(\mu)e^{-\Delta/\mu} + \Lambda^+(0,\mu), \qquad I_p^-(\mu) = I_{p-1}^-(\mu)e^{-\Delta/\mu} + \Lambda^-(\Delta,\mu), \tag{27}$$

where $\Lambda^+(0,\mu)$ is expression (25a) evaluated at $x=0$ and $\Lambda^-(\Delta,\mu)$ is (25b) evaluated at $x=\Delta$. These two relations are applied on a recursive basis to get the upwelling and downwelling intensities at layer boundaries. The downwelling recursion starts at TOA, where the downwelling diffuse intensity is zero ($I_0^-(\mu)=0$).

The starting value for the upwelling recursion is the bottom-of-the-atmosphere (BOA) source term $I_K^+(\mu)$, which may be determined from the surface reflection condition. For a general bi-directionally reflecting surface with albedo R and normalized reflection coefficients $\rho_m^*(\mu,-\mu_j)$ defined for upwelling directions μ, this is:

$$I_K^+(\mu)=(1+\delta_{m0})R\sum_{j=1}^{N}w_j\mu_j\rho_m^*(\mu,-\mu_j)I_{-jK}(\tau_K)+R\mu_0F_\odot\rho_m^*(\mu,-\mu_0)\mathrm{e}^{-\tau_{\mathrm{spher}}(\tau_K)}. \tag{28}$$

This is easy to evaluate since the components $I_{-jK}(\tau_K)$ are known from the discrete ordinate solution for the lowest layer $p=K$. This BOA source term is only present for the $m=0$ Fourier term in the Lambertian case. This result can easily be extended to include surface thermal emission (see SKC for details). Thus to find the upwelling intensity at arbitrary stream angle μ and to arbitrary optical depth τ (assumed to lie within layer q), we start with (28), then use (27) recursively until the lower boundary of layer q is reached. We then apply (24a) once to get the required intensity at τ.

To complete the discrete ordinate solution, we sum the Fourier series (4). It is usual to terminate the azimuth series when the addition of an extra harmonic does not alter the overall intensity by more than a pre-specified relative quantity (the accuracy criterion). This convergence test should be applied to all intensities for which output is desired. Furthermore, it makes sense to apply this test to at least two successive azimuth contributions to avoid accidental omission. This procedure is standard in DISORT [6] and GOMETRAN [7] regarding series convergence.

The *layer-integrated* multiple scatter source term output may be obtained by simply dropping the single scatter contribution from (26):

$$\Lambda_q^{(\mathrm{MS})\pm}(\Delta_q,\mu)=H_q^\pm(\Delta_q,\mu)+D_q^\pm(\Delta_q,\mu) \tag{29}$$

in terms of layer optical thickness Δ_q.

For mean-value (angle-integrated) output, it is only necessary to compute the azimuth-independent term of the Fourier series ($m=0$). Mean value output does not require the above post-processing analysis. The half-space angular integrations are performed using the discrete ordinate quadrature values. Upwelling and downwelling fluxes $\langle F\rangle$ and mean intensities $\langle J\rangle$ at optical depth τ inside the layer p are given by

$$\langle F^+(\tau)\rangle=2\pi\sum_{j=1}^{N}w_j\mu_jI_{jp}^+(\tau)\quad\text{and}\quad\langle F^-(\tau)\rangle=2\pi\sum_{j=1}^{N}w_j\mu_jI_{jp}^-(\tau)+F_\odot\mu_0\mathrm{e}^{-\tau_{\mathrm{spher}}(\tau)}, \tag{30}$$

$$\langle J^+(\tau)\rangle=\frac{1}{2}\sum_{j=1}^{N}w_jI_{jp}^+(\tau)\quad\text{and}\quad\langle J^-(\tau)\rangle=\frac{1}{2}\sum_{j=1}^{N}w_jI_{jp}^-(\tau)+\frac{F_\odot\mu_0}{4\pi}\mathrm{e}^{-\tau_{\mathrm{spher}}(\tau)}, \tag{31}$$

where $I^{\pm}_{jp}(\tau)$ are the discrete ordinate solutions in layer p. Additional direct beam contributions are present in the downwelling case.

3. The pseudo-spherical particular integral

3.1. Direct-beam attenuation in a curved atmosphere

We first discuss the parameterization of the pseudo-spherical source term. In a multi-layer atmosphere, we may write

$$\kappa_q = \sum_{p=1}^{q} \kappa_{qp} = \sum_{p=1}^{q} s_{qp} e_p \tag{32}$$

for the cumulative slant optical depth κ_q to the bottom boundary of layer q in terms of layer path lengths s_{qp}, layer extinctions e_p and slant optical thickness values κ_{qp} for layers p above and equal to q. In a plane-parallel atmosphere, $\kappa_{qp} = \Delta_p/\mu_0$. For straight line paths (shell geometry only) the distances s_{qp} may be expressed easily in terms of vertical altitudes. In a non-refracting atmosphere, κ_q is expressed in terms of the Chapman function [18]. In a refractive atmosphere, s_{qp} can be calculated with repeated application of Snell's law. The zenith solar angle cosine is always $-\mu_0$ for a non-refractive atmosphere. With refractive geometry, one must compute an average value $-\bar{\mu}_{0p}$ for each layer p. In the rest of this paper, we will continue to work with a non-refractive atmosphere, but the analysis is equally valid for the refractive case, provided the above points are noted. To characterize the pseudo-spherical input, we need to specify an input grid of slant path optical depths κ_{qp}, and (for a refractive atmosphere) a local grid of solar zenith cosines $-\bar{\mu}_{0p}$. $\{\kappa_{qp}, -\bar{\mu}_{0p}\}$ are additional inputs to the RT model; in keeping with the philosophy to maintain the generic nature of the discrete ordinate formalism, we do not include ray tracing as part of the model (this should be application-specific).

In a plane-parallel atmosphere, the direct beam attenuation is given by $\exp[-\tau/\mu_0]$. In a curved spherical-shell atmosphere this is replaced by $\exp[-\kappa(\tau)]$. We wish to find a parameterization of this transmittance. The simplest assumption uses an expression which is exact at layer boundaries:

$$\mathrm{e}^{-\kappa(\tau)} \simeq T_q(x) = \hat{T}_q \mathrm{e}^{-x\lambda_q}, \quad \text{where } \hat{T}_q = \mathrm{e}^{-\kappa_{q-1}} \quad \text{and} \quad \lambda_q = \frac{\kappa_q - \kappa_{q-1}}{\Delta_q}. \tag{33}$$

Here, $x = \tau - \tau_{q-1}$ is the partial layer optical thickness. Clearly λ_q is an *average secant factor* which replaces μ_0^{-1} in layer q. Note that this definition is slightly different to that used in [18], where λ_q is defined in terms of the slant path optical depth at the center of the layer. The definition here has the advantage that the attenuation is a continuous function of τ.

This approximation is equivalent to assuming an average attenuation across the layer, and takes no account of variations in optical depth through the layer. Some accuracy is lost for optically thick layers, or for geometrically extensive layers where there is considerable curvature. An improved parameterization may be obtained with the following exponential-sine and exponential-polynomial

expressions:

$$e^{-\kappa(\tau)} \simeq \hat{T}_q e^{-x\lambda_q} \left[1 + \sum_{n=1}^{N_q^*} c_{qn} \sin\left(\frac{nx\pi}{\Delta_q}\right) \right] \tag{34a}$$

$$e^{-\kappa(\tau)} \simeq \hat{T}_q e^{-x\lambda_q} \left[1 + x(\Delta_q - x) \sum_{n=1}^{N_q^*} c_{qn} x^{n-1} \right], \tag{34b}$$

where x, $\hat{T}_q$ and λ_q are defined in (33). In both cases, correct slant path attenuations result at the layer boundaries, and the coefficients c_{qn} may be found by linear fitting, assuming that a suitable number of fine-level attenuation values are available. The number of coefficients N_q^* depends both on the layer optical and geometrical thickness values and on the degree of accuracy desired for the parameterization. In practice, we use a single accuracy measure to ensure that the parameterization is consistently accurate for all layers.

In order to get an idea of the accuracy of these parameterizations, consider a single uniform atmospheric layer L above the ground (lower height level of 0 km), and with varying optical and geometrical thicknesses. We assume that this layer is bounded above by another homogeneous layer of fixed optical thickness 0.25, and extending up to a fixed upper level of 50 km. A non-refractive atmosphere is assumed; the earth radius is 6371 km. We make exact calculations of the attenuation for a large number of subdivisions of L and use these results to find the factors λ_q and T_q and the fitted coefficients c_{qn}. A maximum of 4 coefficients was found to be sufficient in the fitting. Fig. 2 shows the results of these computations for a number of different solar zenith angles (indicated as contours) ranging from 77° to 89.5°. An accuracy criterion of 5% was set for the average secant approximation, and 2% for the other parameterizations. Thus for example in Fig. 2 (center), for all combinations of the ground layer optical and geometric thickness values lying above and to the right of the contour labeled 87°, the exponential-polynomial parameterization will reproduce the solar beam attenuation to better than 2% for a solar zenith angle of 87°. From Fig. 2 (top), a 5% accuracy level for solar zenith angles up to 87° implies that for the average secant approximation, the ground layer optical thickness values should be below $\simeq 0.6$, and corresponding geometrical thickness values should be less than $\simeq 0.6$ km. In practical applications in a multi-layer atmosphere, a sufficient number of layers is used to ensure that inaccuracies in the average secant parameterization due to geometric effects are minimized. However, it is clear that there are limitations on the accuracy of the average secant approximation in the presence of optically thick layers. In Section 5, we give an example of the effect of a more accurate pseudo-spherical parameterization on backscatter intensities at high solar zenith angle.

Finally, we determine the single scatter contributions $E^{\pm}(x, \mu)$ which appeared in the integrated layer source terms (26). The source term to be integrated in this case is $Q^m(\mu)\hat{T}e^{-x\lambda}$ for the average secant pseudo-spherical approximation, where $Q^m(\mu)$ is given by (9) evaluated at zenith cosine μ. Source term integration over optical depth along the lines of (25a) is straightforward. Details are given in Appendix B.2 for all three parameterizations of the direct beam transmittance noted in this section.

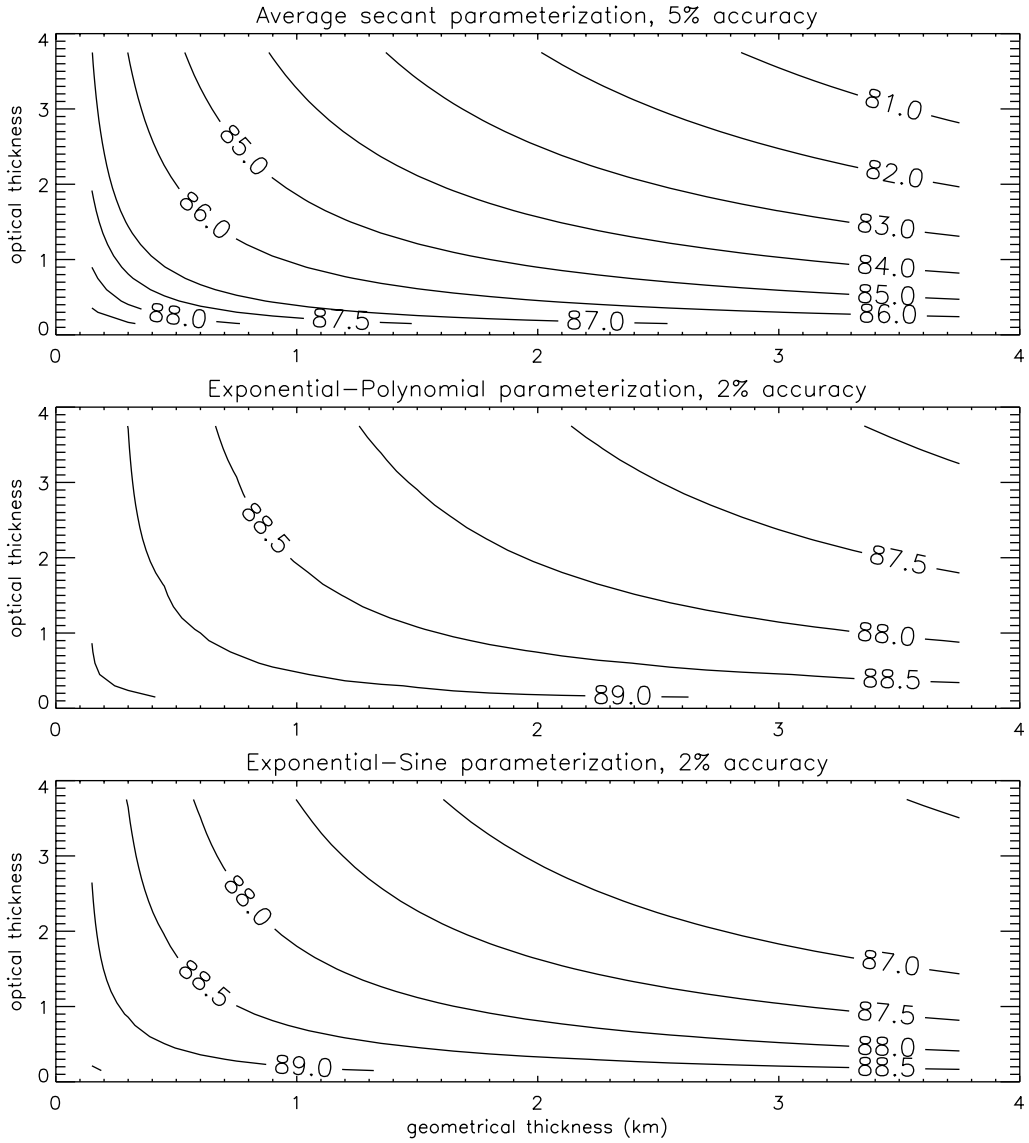

Fig. 2. Direct beam attenuation accuracy; contours label solar zenith angles in (°), so that all geometrical and optical conditions above and right of a given contour indicate that the parameterization is accurate to the specified level for the corresponding solar zenith angle: (top) 5% accuracy levels in the average secant parameterization; (center) 2% accuracy level for the exponential-polynomial parameterization; (bottom) 2% levels for the exponential-sine parameterization.

3.2. *The classical* (*Chandrasekhar*) *particular solution*

We find the particular solution for the average secant approximation. We use a notation similar to that in Section 2.1. For a double-Gauss discrete ordinate scheme with N quadrature abscissae and weights $\{\mu_j, w_j\}$ in the half space, we require the particular solution of the following $2N$ coupled

linear differential equations (we drop the layer index q temporarily):

$$\frac{\mathrm{d}I_i^+}{\mathrm{d}x} = -\sum_{j=1}^{N}\{\zeta_{ij}I_j^+ + \eta_{ij}I_j^-\} - Q_i^+\mu_i^{-1}\hat{T}\mathrm{e}^{-x\lambda} \tag{35a}$$

$$\frac{\mathrm{d}I_i^-}{\mathrm{d}x} = +\sum_{j=1}^{N}\{\eta_{ij}I_j^+ + \zeta_{ij}I_j^-\} + Q_i^-\mu_i^{-1}\hat{T}\mathrm{e}^{-x\lambda}, \tag{35b}$$

where

$$Q_i^{\pm} = (2-\delta_{m0})\frac{F_\odot}{2\pi}\Pi^m(-\mu_0, \pm\mu_i). \tag{36}$$

These expressions are obtained by substituting the average secant form (33) in the general discrete ordinate Eq. (9), and using the definitions of matrices $\boldsymbol{\xi}$ and $\boldsymbol{\eta}$ in (11). For the plane-parallel case, $\lambda = \mu_0^{-1}$ and $\hat{T} = \exp[-\tau_U/\mu_0]$ (τ_U is the upper boundary vertical optical depth). The particular solution $G_j^{\pm}$ is found by substituting $I_j^{\pm} \sim F_j^{\pm}\hat{T}\exp(-x\lambda)$ in (35a) and (35b). This eliminates the optical depth dependence and we are left with a linear system of order $2N$:

$$\lambda F_i^+ = \sum_{j=1}^{N}\{\zeta_{ij}F_j^+ + \eta_{ij}F_j^-\} - Q_i^+\mu_i^{-1}, \tag{37a}$$

$$\lambda F_i^- = -\sum_{j=1}^{N}\{\eta_{ij}F_j^+ - \zeta_{ij}F_j^-\} - Q_i^-\mu_i^{-1}. \tag{37b}$$

If we define sum and difference vectors $\mathbf{H} = \mathbf{F}^+ + \mathbf{F}^-$, $\mathbf{J} = \mathbf{F}^+ - \mathbf{F}^-$, $\mathbf{S} = \mathbf{Q}^+ + \mathbf{Q}^-$ and $\mathbf{D} = \mathbf{Q}^+ - \mathbf{Q}^-$, we can eliminate $\mathbf{J}$ in favor of $\mathbf{H}$, thereby reducing the order of the system from $2N$ to N. The result is

$$(\boldsymbol{\Gamma} - \hat{\mathbf{E}}\lambda^2)\mathbf{H} = -(\boldsymbol{\xi} - \boldsymbol{\eta})\mathbf{S} - \lambda\mathbf{D} \tag{38}$$

for the sum vector $\mathbf{H}$. $\boldsymbol{\Gamma}$ is the eigenmatrix in (10) and $\hat{\mathbf{E}}$ is again the unit matrix. This system is solved numerically by standard means. The difference vector $\mathbf{J}$ is found from the auxiliary equation

$$\lambda\mathbf{J} = (\boldsymbol{\xi} + \boldsymbol{\eta})\mathbf{H} + \mathbf{S} \tag{39}$$

Eqs. (38) and (39) are sufficient to complete the solution. The derivation here (in particular, the reduction in order) follows closely that found in [20].

A similar approach applies to the exponential-polynomial parameterization given in (34b) above. Solutions of the form

$$I_j^{\pm} \sim \hat{T}\mathrm{e}^{-x\lambda}\sum_n F_{jn}^{\pm}x^n \tag{40}$$

may be substituted in the discrete ordinate Eq. (8). Successive powers of x are then equated, and this yields a series of linked linear equations for the components $F_{jn}^{\pm}$ which are solved recursively starting with the highest power of x. A solution for the particular integral in a plane-parallel atmosphere has been developed for an exponential-linear form [23]. For the exponential-sine parameterization (34a), the ansatz $I_j^{\pm} \sim \hat{T}\exp(-x\lambda)\sum_n F_{jn}^{\pm}\sin(nx\pi/\Delta)$ can be used. We will not go into details for the determination of classical solutions for these two parameterizations, as the procedures are somewhat

cumbersome. In the next section we will see that the Green's function technique allows particular solution to be evaluated in a convenient analytic fashion, without the need for solving linear systems numerically.

For integrated particular solution source functions with the classical method, we refer again to the definition in (26), where we now require the particular solution contribution $D^{\pm}_{\mathrm{class}}$. This derivation is given in Appendix B.3. In line with our preference for using the Green's function technique, we do not consider similar expressions for the exponential-sine and exponential-polynomial parameterizations (these will however be derived below in Section 3.3 for the Green's function particular integral contributions).

3.3. The Green's function particular solution

The Green's function method is based on expansions for the upwelling and downwelling particular solution in terms of solution vectors $\mathbf{X}^{(P)}_{\alpha}$ and $\mathbf{X}^{(N)}_{\alpha}$ and separation constants $\pm k_{\alpha}$ for the homogeneous problem. A rigorous derivation of this result is outside the scope of the present paper, but the reader is referred to the explicit formulation of the infinite-medium Green's function found in [26]. The particular form used in the present work assumes that the eigenproblem separation constants occur in pairs, but this is not a necessary requirement. In this section, we summarize the results given in [20]. We write

$$G^{+}_{j}(\tau) = \sum_{\alpha=1}^{N} \{A_{\alpha}(\tau) X^{(P)}_{j\alpha} + B_{\alpha}(\tau) X^{(N)}_{j\alpha}\}, \quad G^{-}_{j}(\tau) = \sum_{\alpha=1}^{N} \{A_{\alpha}(\tau) X^{(N)}_{j\alpha} + B_{\alpha}(\tau) X^{(P)}_{j\alpha}\} \tag{41}$$

for the upwelling $(+)$ and downwelling $(-)$ particular integral solutions $G^{\pm}_{j}(x)$ of (8), where the multipliers A and B are given by

$$A_{\alpha}(\tau) = a_{\alpha} C^{-}_{\alpha}(\tau) \quad \text{and} \quad B_{\alpha}(\tau) = b_{\alpha} C^{+}_{\alpha}(\tau). \tag{42}$$

In (42), the terms independent of optical depth are given by

$$a_{\alpha} = \frac{1}{N_{\alpha}} \sum_{j=1}^{N} w_j [P^{-}_{j} X^{(N)}_{j\alpha} + P^{+}_{j} X^{(P)}_{j\alpha}], \quad b_{\alpha} = \frac{1}{N_{\alpha}} \sum_{j=1}^{N} w_j [P^{+}_{j} X^{(N)}_{j\alpha} + P^{-}_{j} X^{(P)}_{j\alpha}], \tag{43}$$

where the normalization factor N_{α} is given by

$$N_{\alpha} = \sum_{j=1}^{N} \mu_j w_j [X^{(N)}_{j\alpha} X^{(N)}_{j\alpha} - X^{(P)}_{j\alpha} X^{(P)}_{j\alpha}] \tag{44}$$

and $P^{\pm}_{j} = (2 - \delta_{m0}) \Pi^{m}(\pm\mu_j, -\mu_0)$ (the Π function was defined in (7)). If the layer upper and lower optical depths are τ_{U} and τ_{L} respectively, then the *optical depth multipliers* in (42) are given by

$$C^{-}_{\alpha}(\tau) = \int_{\tau_{\mathrm{U}}}^{\tau} \mathrm{e}^{-k_{\alpha}(\tau - y)} \mathrm{e}^{-\tau_{\mathrm{spher}}(y)} \, \mathrm{d}y \quad \text{and} \quad C^{+}_{\alpha}(\tau) = \int_{\tau}^{\tau_{\mathrm{L}}} \mathrm{e}^{-k_{\alpha}(y - \tau)} \mathrm{e}^{-\tau_{\mathrm{spher}}(y)} \, \mathrm{d}y. \tag{45}$$

These results may be verified by substituting (41) in the discrete ordinate RTE (8) and using (42) and (43) together with the properties of the eigensolutions to separate the optical depth dependence and construct the multipliers in (45). The most important property of these eigensolutions is their full-range orthogonality. We note that the particular integral is written in analytic form, requiring

only the evaluation of the optical depth integrals (45). Results for $C_\alpha^\pm(\tau)$ in a plane-parallel medium have been noted several times in the literature (see for example [26] or [20]). Since the average secant parameterization is in fact a local plane-parallel formulation with $e^{-\tau_{\rm spher}(y)} \simeq \hat{T} e^{-(y-\tau_U)\lambda}$, the integrals in (45) are straightforward:

$$C_\alpha^-(x) = \hat{T}\frac{e^{-xk_\alpha} - e^{-x\lambda}}{\lambda - k_\alpha} \quad \text{and} \quad C_\alpha^+(x) = \hat{T}\frac{e^{-x\lambda} - e^{-\Delta\lambda}e^{-(\Delta-x)k_\alpha}}{\lambda + k_\alpha}, \tag{46}$$

where again, $x = \tau - \tau_U$ and $\Delta = \tau_L - \tau_U$. In Appendix A we calculate optical depth multipliers for the exponential-polynomial and exponential-sine parameterizations.

For the post-processing function, we refer to (26) and write $D^\pm_{\rm Green}(x,\mu)$ for the integrated particular solution contribution to the partial-layer source terms. In Appendix B.4, we present derivations of $D^\pm_{\rm Green}$ for all three parameterizations of the direct beam transmittance considered in this paper.

The Green's function method offers a more systematic way of dealing with parameterizations of the direct beam. In general, the classical method (which relies on substitution) is limited to source terms with straightforward and separable dependence on optical depth; the Green's function formalism is more powerful and offers greater scope for dealing with a wider variety of source terms.

4. Linearization of the pseudo-spherical discrete ordinate solution

4.1. Preamble: linearization rules

In the previous work (SKC), a perturbation analysis of the intensity field in a plane-parallel multi-layer multiply scattering atmosphere was carried out in order to establish analytical weighting functions. In this paper, we adopt a slightly different emphasis, instead working directly with the partial derivatives of the discrete ordinate solution components. Since the discrete ordinate RTE comprises a set of coupled *linear* first-order differential equations, this is equivalent to the perturbation analysis. We also extend the analysis in two directions: (1) the derivation of weighting functions for the pseudo-spherical model, and (2) the generalization to upwelling and downwelling output at arbitrary stream angles and optical depth. Together this enables weighting functions to be calculated for any atmospheric application, in addition to extending the range of viewing geometries to include large solar zenith angle scenarios.

In order to generate weighting functions with respect to any given atmospheric parameter, we require the corresponding variational derivatives of the basic optical property inputs to the RTE. We consider variations only of layer single-scatter albedo and extinction coefficient, though it is possible to consider variations of the phase function moments. Consider an atmospheric parameter ξ_q in layer q; the relative (parameter-normalized) weighting function definition is:

$$\mathscr{K}_{\xi_q}(\tau,\mu,\phi_0-\phi) = \sum_{m=0}^{2N-1} \mathscr{K}^m_{\xi_q}(\tau,\mu)\cos m(\phi_0-\phi), \tag{47}$$

$$\mathscr{K}^m_{\xi_q}(\tau,\mu) = \mathscr{L}_{\xi_q}[I^m(\tau,\mu)] = \xi_q \frac{\partial I^m(\tau,\mu)}{\partial \xi_q}. \tag{48}$$

Eq. (48) defines the *linearization operator* $\mathscr{L}_\xi = \xi\partial/\partial\xi$, and we will continue to use this notation in the weighting function analysis.

The input variational quantities that determine the weighting functions may be expressed as

$$\{u_q, v_q\} = \left\{ \frac{\mathscr{L}_q[\omega_q]}{\omega_q}, \frac{\mathscr{L}_q[e_q]}{e_q} \right\} = \left\{ \frac{\xi_q}{\omega_q} \frac{\partial \omega_q}{\partial \xi_q}, \frac{\xi_q}{e_q} \frac{\partial e_q}{\partial \xi_q} \right\}. \tag{49}$$

Here, u_q can be thought of as the *relative change* in single scattering albedo ω_q induced by a relative change in property ξ_q, and v_q as the *relative change* in extinction coefficient e_q induced by a relative change in ξ_q. The pairs $\{u_q, v_q\}$ are fundamental to the weighting function derivation, and they will be established beforehand and entered as additional inputs to LIDORT.

A simple example will illustrate the construction of the optical properties and their derivatives. Consider a single homogeneous layer of depth h with Rayleigh (molecular) scattering and absorption by one trace gas species g. The single scattering albedo is $\omega = \sigma_{\text{Ray}}/\sigma_{\text{total}}$, where $\sigma_{\text{total}} = \sigma_{\text{Ray}} + X_g\sigma_g$, σ_{Ray} is the Rayleigh cross section, σ_g the trace gas absorption cross section, and X_g the trace gas volume mixing ratio. The layer extinction coefficient is $e = \sigma_{\text{total}}\rho_{air}$, and the vertical optical thickness is $\Delta = eh$, where ρ_{air} is the air number density (assumed constant). If $\xi = X_g$ is the property undergoing variation, it can be shown readily that

$$u_\xi = -\frac{X_g\sigma_g}{\sigma_{\text{Ray}} + X_g\sigma_g} \quad \text{and} \quad v_\xi = +\frac{X_g\sigma_g}{\sigma_{\text{Ray}} + X_g\sigma_g}. \tag{50}$$

In the Earth's atmosphere, there are normally at least two scatterers (molecules and aerosols, where the latter may include clouds). For each particulate s in layer q, we have single scattering albedos ω_{qs} and phase function moment coefficients β_{lqs}. Each single scattering albedo is normalized to the total extinction coefficient. Then we have $\omega_q = \sum_s \omega_{qs}$, and the combination $\omega_q\beta_{lq}$ which appears in the equations in Sections 2 and 3 is defined by the sum $\sum_s \omega_{qs}\beta_{lqs}$ over particulates. β_{lq} is a weighted mean value of the separate moment coefficients β_{lqs}. For the linearization, we also have relative derivatives u_{qs} defined for each scatterer s. Continuing to use these definitions of ω_q and β_{lq}, it is necessary to define weighted mean values u_{lq} such that $\omega_q\beta_{lq}u_{lq} = \sum_s \beta_{lqs}\omega_{qs}u_{qs}$. This is the combination that appears in the linearization analysis.

In a multi-layer atmosphere, it is important to note that variations in parameter ξ_q in layer q will affect all *cumulative* vertical optical depths τ in and below that layer. For layers below q, the variation in τ is $\Delta_q v_q$, since the optical thickness of layer q will undergo variation by this amount, but optical thicknesses for all layers below q are not affected. This observation applies equally to slant path optical depth values, since layer slant optical thicknesses are also proportional to extinction coefficients. Summarizing, we may write down the rules for the linearization analysis:

$$\mathscr{L}_q[\tau] = \begin{cases} xv_q & \text{for } \tau_{q-1} < \tau < \tau_q, \\ 0 & \text{for } \tau \leqslant \tau_{q-1}, \\ \Delta_q v_q & \text{for } \tau \geqslant \tau_q, \end{cases} \tag{51a}$$

$$\mathscr{L}_q[\omega_p] = \begin{cases} u_q\omega_q & \text{for } q = p, \\ 0 & \text{for } q \neq p \end{cases} \tag{51b}$$

for $x = \tau - \tau_{q-1}$ and $\Delta_q = \tau_q - \tau_{q-1}$.

Now we examine the linearization of the direct beam attenuation. From (32), it follows that $\mathscr{L}_q[\kappa_p] = v_q\kappa_{pq}$, and from the definition (33) of the average secant parameterization, we obtain:

$$\mathscr{L}_q[\hat{T}_p] = -v_q\kappa_{p-1,q}\hat{T}_p \quad \text{for } q < p, \quad \mathscr{L}_q[\hat{T}_p] = 0 \quad \text{for } q \geqslant p \tag{52}$$

with

$$\Delta_p \mathscr{L}_q[\lambda_p] = \begin{cases} -v_q(\kappa_{pq} - \kappa_{p-1,q}) & \text{for } q < p \text{ and } p > 1, \\ -v_q(\kappa_{pq} - \Delta_p \lambda_p) & \text{for } q = p, \\ 0 & \text{for } q > p. \end{cases} \tag{53}$$

Bringing these results together, we find

$$\Delta_p \mathscr{L}_q[T_p(x)] = \begin{cases} -v_q[\kappa_{pq}(\Delta_p - x) - \kappa_{p-1,q}x]T_p(x) & \text{for } q < p \quad \text{and } p > 1, \\ -v_q\kappa_{pq}xT_p(x) & \text{for } q = p, \\ 0 & \text{for } q > p. \end{cases} \tag{54}$$

These results are vital for the linearization analysis of the particular integral, and we will need them later. For the plane-parallel (pp) case, we have $\lambda_p = \mu_0^{-1}$ and $\kappa_{pq} = \Delta_p \mu_0^{-1}$, and hence

$$\mu_0 \mathscr{L}_q[T_p^{(pp)}(x)] = \begin{cases} -v_q \Delta_q T_p^{(pp)}(x) & \text{for } q < p, \\ -v_q x T_p^{(pp)}(x) & \text{for } q = p, \\ 0 & \text{for } q > p. \end{cases} \tag{55}$$

The plane-parallel result was derived in a different form in SKC; the average secant result is new.

In Section 4.2 we go through the linearization process for the discrete ordinate homogeneous solutions; this mirrors the treatment in SKC. Sections 4.3 and 4.4 deal with the linearization of the classical and Green's function particular integrals, with particular emphasis paid to the effects of the pseudo-spherical assumption. The analysis for the particular solutions is restricted to the average secant parameterization. The linearization of the boundary value problem follows in Section 4.5; the treatment is more general than the plane-parallel analysis presented in SKC. In Section 4.6 we examine the post-processing function in order to establish linearizations (and hence weighting functions) at arbitrary optical depth and stream angle, again paying particular attention to the pseudo-spherical treatment.

Note also that one can define an albedo weighting function: $\mathscr{K}_R(\tau, \mu) = R\partial I(\tau, \mu)/\partial R$. For a Lambertian surface, this weighting function is only nonzero for the azimuth-independent Fourier term. Layer homogeneous and particular solutions do not depend on the albedo, so their partial derivatives with respect to R vanish. The albedo only appears explicitly in the surface boundary condition BC3, so the corresponding linearization operator $\mathscr{L}_R$ need only be applied to this result. We note this development in Section 4.5, and mention the post-processing function for albedo weighting functions in Section 4.6. The notion of an albedo weighting function can easily be extended to a more general surface reflectance condition, if we assume no sensitivity to the shape of the bi-directional reflectance function.

The analysis presented here is restricted to a solar beam source; we do not consider weighting functions with respect to sources of atmospheric thermal emission. However, the latter was done in SKC, where thermal emission was assumed isotropic, and the results established in that work can easily be incorporated in the present analysis.

4.2. Linearization analysis for the homogeneous solutions

We assume that derivatives $\{u_q, v_q\}$ have been defined with respect to property ξ varying in layer q. We drop the index q for now, since derivatives with respect to ξ vanish for homogeneous solutions in layers other than q. If x is the optical thickness measured from the top boundary of

the layer, and Δ the thickness for the whole layer, then as noted above, $\mathscr{L}[x] = xv$ and $\mathscr{L}[\Delta] = \Delta v$. The homogeneous solutions are $\mathbf{X}_\alpha^{(P)} e^{-k_\alpha x}$ and $\mathbf{X}_\alpha^{(N)} e^{-k_\alpha(\Delta - x)}$. Applying the linearization operation and using the chain rule gives us:

$$\mathscr{L}[\mathbf{X}_\alpha^{(P)} e^{-k_\alpha x}] = e^{-k_\alpha x}\{\mathscr{L}[\mathbf{X}_\alpha^{(P)}] - (\mathscr{L}[k_\alpha] + vk_\alpha)x\mathbf{X}_\alpha^{(P)}\}, \tag{56}$$

$$\mathscr{L}[\mathbf{X}_\alpha^{(N)} e^{-k_\alpha(\Delta - x)}] = e^{-k_\alpha(\Delta - x)}\{\mathscr{L}[\mathbf{X}_\alpha^{(N)}] - (\mathscr{L}[k_\alpha] + vk_\alpha)(\Delta - x)\mathbf{X}_\alpha^{(N)}\}. \tag{57}$$

To determine $\mathscr{L}[k_\alpha]$ and $\mathscr{L}[\mathbf{X}_\alpha]$, we apply the linearization operator to the eigenvalue problem (10). We note first that the elements Π_{ij} in the definitions of $\boldsymbol{\xi}$ and $\boldsymbol{\eta}$ in (11) are proportional to ω, so that $\mathscr{L}[\Pi_{ij}] = u\Pi_{ij}$. It follows that:

$$\mathscr{L}[\Gamma_{ij}] = u\sum_{l=1}^{N}\left\{\frac{w_l C_{il}^-}{\mu_i}(\zeta_{lj} + \eta_{lj}) + (\zeta_{il} - \eta_{il})\frac{w_j C_{lj}^+}{\mu_l}\right\}, \quad \text{where } C_{ij}^\pm = \mathbf{\Pi}_{ij}^+ \pm \mathbf{\Pi}_{ij}^-. \tag{58}$$

The linearization of (10) gives:

$$\sum_{j=1}^{N}(\Gamma_{ij} - \delta_{ij}k_\alpha^2)\mathscr{L}[\varsigma_{j\alpha}] = 2k_\alpha\mathscr{L}[k_\alpha]\varsigma_{i\alpha} + \sum_{l=1}^{N}\mathscr{L}[\Gamma_{ij}]\varsigma_{j\alpha}. \tag{59}$$

Since for each α there are $N+1$ unknowns $\mathscr{L}[k_\alpha]$ and $\mathscr{L}[\varsigma_{i\alpha}]$, $i = 1,\ldots,N$, an additional condition is required in order to find the solution. This comes from the unit normalization condition imposed on the eigenvectors. Since $\boldsymbol{\varsigma}_\alpha \cdot \boldsymbol{\varsigma}_\alpha = 1$ (vector product), then it follows that $\mathscr{L}[\boldsymbol{\varsigma}_\alpha] \cdot \boldsymbol{\varsigma}_\alpha = 0$. Together with (59), we get the combined linear system $\mathbf{M}_\alpha \mathbf{\Xi}_\alpha = \mathbf{B}_\alpha$, where vectors $\mathbf{\Xi}_\alpha$ and $\mathbf{B}_\alpha$ and matrix $\mathbf{M}_\alpha$ are given by:

$$\mathbf{\Xi}_\alpha = \begin{bmatrix} \mathscr{L}[k_\alpha] \\ \mathscr{L}[\varsigma_{1\alpha}] \\ \mathscr{L}[\varsigma_{2\alpha}] \\ \vdots \\ \mathscr{L}[\varsigma_{N\alpha}] \end{bmatrix}, \qquad \mathbf{B}_\alpha = \begin{bmatrix} \sum_j \xi_{1j}\varsigma_{j\alpha} \\ \sum_j \xi_{2j}\varsigma_{j\alpha} \\ \vdots \\ \sum_j \xi_{Nj}\varsigma_{j\alpha} \\ 0 \end{bmatrix},$$

$$\mathbf{M}_\alpha = \begin{bmatrix} 2k_\alpha\varsigma_{1\alpha} & k_\alpha^2 - \Gamma_{11} & -\Gamma_{12} & \cdots & -\Gamma_{1N} \\ 2k_\alpha\varsigma_{2\alpha} & -\Gamma_{21} & k_\alpha^2 - \Gamma_{22} & \cdots & -\Gamma_{2N} \\ \vdots & \vdots & \vdots & \ddots & \vdots \\ 2k_\alpha\varsigma_{N\alpha} & -\Gamma_{N1} & -\Gamma_{N2} & \cdots & k_\alpha^2 - \Gamma_{NN} \\ 0 & \varsigma_{1\alpha} & \varsigma_{2\alpha} & \cdots & \varsigma_{N\alpha} \end{bmatrix}. \tag{60}$$

Solving this system gives us $\mathscr{L}[k_\alpha]$ and $\mathscr{L}[\varsigma_\alpha]$. We now linearize the auxiliary Eq. (12) to find $\mathscr{L}[\vartheta_\alpha]$. From these results, the linearizations $\mathscr{L}[\mathbf{X}_\alpha^{(P)}]$ and $\mathscr{L}[\mathbf{X}_\alpha^{(N)}]$ may be obtained; these have the same symmetry properties (14) as the original solution vectors. Reintroducing layer indices, we note that for $q \neq p$, $\mathscr{L}_q[k_{p\alpha}] = 0$, $\mathscr{L}_q[\mathbf{X}_{p\alpha}^{(P)}] = 0$ and $\mathscr{L}_q[\mathbf{X}_{p\alpha}^{(P)}] = 0$. These results were derived in SKC using perturbation methods.

4.3. Linearization analysis for the classical particular solution

In this section, we retain the layer indices. We derive the linearization only for the average secant parameterization of the direct beam transmittance. The original particular solution in a given layer q was determined from the linear system (38), so that application of the linearization operator $\mathscr{L}_q$ will result in the same linear system with a different source vector. From the previous section, we know the linearizations $\mathscr{L}_q[\mathbf{\Gamma}_q]$, $\mathscr{L}_q[\boldsymbol{\xi}_q]$ and $\mathscr{L}_q[\boldsymbol{\eta}_q]$; all these matrices are linearly proportional to ω_q, so their linearizations depend only on u_q. Further, $\mathscr{L}_q[\mathbf{\Gamma}_p] = 0$ for $q \neq p$, and similarly for $\boldsymbol{\xi}_p$ and $\boldsymbol{\eta}_p$. Secondly, we have $\mathscr{L}_q[\mathbf{S}_q] = u_q\mathbf{S}_q$ and $\mathscr{L}_q[\mathbf{D}_q] = u_q\mathbf{D}_q$, since $\mathbf{S}_q = \mathbf{Q}_q^+ + \mathbf{Q}_q^-$, $\mathbf{D}_q = \mathbf{Q}_q^+ - \mathbf{Q}_q^-$ and $\mathbf{Q}_q^\pm$ as defined in (36) all vary with ω_q. Again there is no variation of these quantities for $q \neq p$. With these considerations in mind, we can now apply the linearization operator directly to (38). The result for the pseudo-spherical case is:

$$(\mathbf{\Gamma}_p - \hat{\mathbf{E}}\lambda_p^2)\mathscr{L}_q[\mathbf{H}_p] = \delta_{pq}\mathbf{Z}_q + (2\lambda_p\mathbf{H}_p - \mathbf{D}_p)\mathscr{L}_q[\lambda_p], \tag{61}$$

where

$$\mathbf{Z}_q = -\mathscr{L}_q[\boldsymbol{\xi}_q - \boldsymbol{\eta}_q]\mathbf{S}_q - (\boldsymbol{\xi}_q - \boldsymbol{\eta}_q)\mathscr{L}_q[\mathbf{S}_q] - \lambda_q\mathscr{L}_q[\mathbf{D}_q] - \mathscr{L}_q[\mathbf{\Gamma}_q]\mathbf{H}_q. \tag{62}$$

This result is valid for $p \geqslant q$. (The plane-parallel result is considerably simpler: only the term $\delta_{pq}\mathbf{Z}_q$ is present, since $\mathscr{L}_q[\lambda_p] = 0$ for $\lambda_p = \mu_0^{-1}$ a constant; it follows that $\mathscr{L}_q[\mathbf{H}_p] = 0$ for $p \neq q$ in this case.) It is clear from (61) that the solutions $\mathscr{L}_q[\mathbf{H}_p]$ are determined using the same matrices $\mathbf{\Gamma}_p - \hat{\mathbf{E}}\lambda_p^2$ that were used in the original system (38). Since we have already inverted these matrices while solving for the original vectors $\mathbf{H}_p$, the linearizations follow by back-substitution.

In a similar vein, we can linearize the auxiliary Eq. (39) to find $\mathscr{L}_q[\mathbf{J}_p]$:

$$\lambda_p\mathscr{L}_q[\mathbf{J}_p] = -\mathbf{J}_p\mathscr{L}_q[\lambda_p] + (\boldsymbol{\xi}_p + \boldsymbol{\eta}_p)\mathscr{L}_q[\mathbf{H}_p] + \delta_{pq}\mathbf{Z}_q, \tag{63}$$

where this time the auxiliary vector $\mathbf{Z}_q$ is given by

$$\mathbf{Z}_q = \mathscr{L}_q[\boldsymbol{\xi}_q + \boldsymbol{\eta}_q]\mathbf{H}_q. \tag{64}$$

This result is valid for $p \geqslant q$ in the pseudo-spherical case. (In the plane-parallel case, $\mathscr{L}_q[\mathbf{J}_p] = 0$ for $p \neq q$). Eqs. (61)–(64) are sufficient to determine the linearizations $\mathscr{L}_q[\mathbf{F}_p^\pm]$ in the definition of the particular solution. Since the particular solutions themselves are given by $\mathbf{G}_p^\pm(x) = \mathbf{F}_p^\pm T_p(x)$, where $T_p(x) = \hat{T}_p\mathrm{e}^{-x\lambda_p}$, we can now write down the complete result for the linearization of $\mathbf{G}_p^\pm$:

$$\mathscr{L}_q[\mathbf{G}_p^\pm(x)] = \mathscr{L}_q[\mathbf{F}_p^\pm]T_q(x) + \mathbf{F}_p^\pm\mathscr{L}_q[T_p(x)] \quad \text{for } p \geqslant q, \tag{65}$$

where $\mathscr{L}_q[T_p(x)]$ is given by (54).

4.4. Linearization analysis for the Green's function particular solution

In this section we carry out a linearization analysis on the Green's function solution. We retain layer indices throughout. In (43), $a_{p\alpha}$ is independent of optical depth, so that $\mathscr{L}_q[a_{p\alpha}]=0$ for $p\neq q$, and similarly for the other terms defined in (43) and (44). We proceed by applying the linearization operator to (41) and using the chain rule:

$$\mathscr{L}_q[G^+_{jp}(x)] = \sum_{\alpha=1}^{N} \{\mathscr{L}_q[A_{p\alpha}(\tau)]X^{(P)}_{jp\alpha} + \mathscr{L}_q[B_{p\alpha}(\tau)]X^{(N)}_{jp\alpha}\} + \delta_{pq}Z_{jq} \tag{66}$$

where now

$$Z_{jq} = \sum_{\alpha=1}^{N} \{A_{q\alpha}(\tau)\mathscr{L}_q[X^{(P)}_{jp\alpha}] + B_{q\alpha}(\tau)\mathscr{L}_q[X^{(N)}_{jp\alpha}]\} \tag{67}$$

with a similar result for $\mathscr{L}_q[G^-_{jp}(x)]$. The linearizations of $\mathbf{X}^{(P)}_{p\alpha}$ and $\mathbf{X}^{(N)}_{p\alpha}$ are known from Section 4.2. Further, we have from (42)

$$\mathscr{L}_q[A_{p\alpha}(\tau)] = \delta_{pq}\mathscr{L}_q[a_{p\alpha}]C^+_{p\alpha}(\tau) + a_{p\alpha}\mathscr{L}_q[C^+_{p\alpha}(\tau)] \tag{68}$$

and similarly for $\mathscr{L}_q[B_{p\alpha}(\tau)]$. From the definition (43) for $a_{p\alpha}$, we find

$$\mathscr{L}_q[a_{q\alpha}] = \frac{a_{q\alpha}}{N_{q\alpha}}\{u_q N_{q\alpha} - \mathscr{L}_q[N_{q\alpha}]\} + \frac{1}{N_{q\alpha}}\sum_{j=1}^{N} w_j\{Q^-_{jq}\mathscr{L}_q[X^{(N)}_{jq\alpha}] + Q^+_{jq}\mathscr{L}_q[X^{(P)}_{jq\alpha}]\} \tag{69}$$

and similarly for $\mathscr{L}_q[b_{q\alpha}]$. In deriving this result we used the fact that $\mathscr{L}_q[Q^{\pm}_{jq}] = u_q Q^{\pm}_{jq}$. For the linearization of the normalization factor $N_{q\alpha}$ in (44), we obtain

$$\mathscr{L}_q[N_{q\alpha}] = 2\sum_{j=1}^{N} \mu_j w_j\{X^{(N)}_{j\alpha}\mathscr{L}_q[X^{(N)}_{jq\alpha}] - X^{(P)}_{j\alpha}\mathscr{L}_q[X^{(P)}_{jq\alpha}]\}. \tag{70}$$

In dealing with the linearizations of the optical depth multipliers in (46), we must distinguish between those multipliers in the layer q in which the variation in parameter ξ_q is taking place, and multipliers in layers $p>q$ which will be affected by the variation in layer q. Using the fact that $\mathscr{L}_q[\Delta_p] = \Delta_q v_q \delta_{pq}$ and $\mathscr{L}_q[x] = x v_q \delta_{pq}$ for x in q, and the result already established in Section 4.2 for $\mathscr{L}_q[k_{q\alpha}]$, we find

$$\mathscr{L}_q[C^+_{p\alpha}(x)] = \frac{\hat{T}_p}{\lambda_p - k_{p\alpha}}\{-\mathrm{e}^{-x\lambda_p}x\chi_{pq} + \mathrm{e}^{-\Delta_p\lambda_p}\mathrm{e}^{-(\Delta_p - x)k_{p\alpha}}\psi_{pq\alpha}\} + \varpi^+_{pq\alpha}C^+_{p\alpha}(x), \tag{71}$$

$$\mathscr{L}_q[C^-_{p\alpha}(x)] = \frac{\hat{T}_p}{\lambda_p + k_{p\alpha}}\{-\mathrm{e}^{-xk_{p\alpha}}\delta_{pq}x\gamma_{q\alpha} + \mathrm{e}^{-x\lambda_p}x\chi_{pq}\} + \varpi^-_{pq\alpha}C^-_{p\alpha}(x), \tag{72}$$

where

$$\gamma_{q\alpha} = \mathscr{L}_q[k_{q\alpha}] + v_q k_{q\alpha}, \tag{73}$$

$$\chi_{pq} = \delta_{pq}v_q\lambda_p + \mathscr{L}_q[\lambda_p], \tag{74}$$

$$\varpi_{pq\alpha}^{\pm} = \frac{\mathscr{L}_q[\hat{T}_p]}{\hat{T}_p} \mp \frac{\mathscr{L}_q[\lambda_p] \mp \delta_{pq}\mathscr{L}_q[k_{q\alpha}]}{\lambda_p \mp k_{p\alpha}} \tag{75}$$

and

$$\psi_{pq\alpha} = \Delta_p \varpi_{pq\alpha}^{+} + \delta_{pq}(\Delta_p - x)\gamma_{q\alpha}. \tag{76}$$

Again this is valid for $p \geqslant q$. This completes the linearization of the Green's function solution.

4.5. Linearization analysis of the boundary value problem

This is one of the most important aspects of the weighting function analysis. Applying the linearization operator to the boundary conditions will determine the linearizations $\mathscr{L}_q[L_{p\alpha}]$ and $\mathscr{L}_q[M_{p\alpha}]$ for the integration constants $L_{p\alpha}$ and $M_{p\alpha}$ in (16) in terms of the linearizations worked out in the previous three sub-sections for the component homogeneous and particular solutions. We first apply the chain rule to (16) in layer p:

$$\mathscr{L}_q[I_{jp}] = \sum_{\alpha=1}^{N} \{\mathscr{L}_q[L_{p\alpha}]X_{jp\alpha}^{(P)}\mathrm{e}^{-k_{p\alpha}} + \mathscr{L}_q[M_{p\alpha}]X_{jp\alpha}^{(N)}\mathrm{e}^{-k_{p\alpha}(\Delta_p - x)}\} + \mathscr{L}_q[G_{jp}] + \delta_{pq}\mathscr{L}_q[Z_{jq}], \tag{77}$$

where some of the dependence on x has been suppressed for convenience. The last term is only present when $p = q$ and is given by

$$\mathscr{L}_q[Z_{jq}] = \sum_{\alpha=1}^{N} \{L_{q\alpha}\mathscr{L}_q[X_{jq\alpha}^{(P)}\mathrm{e}^{-k_{q\alpha}x}] + M_{q\alpha}\mathscr{L}_q[X_{jq\alpha}^{(N)}\mathrm{e}^{-k_{q\alpha}(\Delta_q - x)}]\}. \tag{78}$$

We can now apply the linearization operator to the three boundary conditions BC1, BC2 and BC3 as written down in Section 2.3. Clearly the linearization $\mathscr{L}_q[I_{jp}]$ must also satisfy these conditions (in terms of the perturbation analysis in SKC, the perturbed field also obeys the same conditions). Using the notation developed earlier for the boundary conditions for the intensity problem, we can write down explicit equations for these boundary conditions, noting that x takes values only at the layer boundaries (that is, $x = 0$ or $x = \Delta_p$ for layer p). We use indices p and r to label layers, while q is reserved for the layer that contains a varying parameter. By analogy with (19), (21) and (22), we have

$$\sum_{\alpha=1}^{N} \{\mathscr{L}_q[L_{p\alpha}]X_{-jp\alpha}^{(P)} + \mathscr{L}_q[M_{p\alpha}]\Theta_{p\alpha}X_{-jp\alpha}^{(N)}\} = B_{jp}^{(1)}, \tag{79a}$$

$$\sum_{\alpha=1}^{N} [\{\mathscr{L}_q[L_{r\alpha}]\Theta_{r\alpha}X_{jr\alpha}^{(P)} + \mathscr{L}_q[M_{r\alpha}]X_{jr\alpha}^{(N)}\} - \{\mathscr{L}_q[L_{p\alpha}]X_{jp\alpha}^{(P)} + \mathscr{L}_q[M_{p\alpha}]\Theta_{p\alpha}X_{jp\alpha}^{(N)}\}] = B_{jp}^{(2)}, \tag{79b}$$

$$\sum_{\alpha=1}^{N} \{\mathscr{L}_q[L_{p\alpha}]\Theta_{p\alpha}\Phi_{j\alpha}^{(P)} + \mathscr{L}_q[M_{p\alpha}]\Phi_{j\alpha}^{(N)}\} = B_{jp}^{(3)}. \tag{79c}$$

The right-hand side vectors are

$$B_{jp}^{(1)} = -\{\mathscr{L}_q[G_{-jp}] + \delta_{pq}\mathscr{L}_q[Z_{-jp}]\}|_{\tau_0}, \tag{80a}$$

$$B_{jp}^{(2)} = \{(\mathscr{L}_q[G_{jp}] - \mathscr{L}_q[G_{jr}]) + (\delta_{pq}\mathscr{L}_q[Z_{jp}] - \delta_{rq}\mathscr{L}_q[Z_{jr}])\}|_{\tau_r}, \tag{80b}$$

$$B_{jp}^{(3)} = R\mu_0 F_\odot \mathscr{L}_q[\hat{T}_p \mathrm{e}^{-\Delta_p \lambda_p}] - \mathscr{L}_q[\Psi_j] - \delta_{pq}\mathscr{L}_q[Y_{jp}]. \tag{80c}$$

In (79a) and (79c), $j = 1,\ldots,N$, and $-j$ denotes the downwelling stream directions. In (79b), $j = \pm 1,\ldots,\pm N$. On the right hand sides, the vectors B are evaluated at the optical depths indicated; $p=1$ in (79a), $r=p-1$ in (79b) and $p=K$ in (79c). The transmittance factors $\Theta_{p\alpha}$ have been defined in (20), vectors $\mathbf{\Phi}^{(P)}$ and $\mathbf{\Phi}^{(N)}$ in (23a), and $\mathbf{\Psi}$ in (23b). The BC3 condition was written down for a Lambertian surface in (80c), but the generalization to a bi-directional surface is straightforward. There is one additional definition in (80c), namely

$$\mathscr{L}_q[Y_{jq}] = \sum_{\alpha=1}^{N} \{L_{q\alpha}\mathscr{L}_q[\Phi_{j\alpha}^{(P)}\Theta_{p\alpha}] + M_{q\alpha}\mathscr{L}_q[\Phi_{jq\alpha}^{(N)}]\}. \tag{81}$$

It is seen immediately that these conditions provide a linear system similar to that used to solve the original boundary value problem. Indeed the solution matrix $\mathscr{A}$ in Section 2.3 is the same as before, so we can write $\mathscr{A}\,\mathscr{L}_q[\mathscr{X}] = \mathscr{L}_q[\mathscr{B}]$, where the vector $\mathscr{L}_q[\mathscr{X}]$ consists of the set of unknown linearized integration constants $\mathscr{L}_q[L_{p\alpha}]$ and $\mathscr{L}_q[M_{p\alpha}]$, and the solution vector $\mathscr{L}_q[\mathscr{B}]$ is constructed from the expressions (80a), (80b) and (80c). Since we have already found the inverse of $\mathscr{A}$ while solving the original boundary value problem, it is straightforward to determine the vector $\mathscr{L}_q[\mathscr{X}]$ by back-substitution. No additional matrix inversion is required, and the results are analytic, depending only on the accuracy with which the original intensity was calculated. The formulation presented here is slightly different from that in SKC, where a more explicit breakdown of the boundary conditions was presented in a plane-parallel multilayer atmosphere.

For the albedo weighting function, the discrete ordinate homogeneous and particular solutions have no partial derivatives, and we need only find $\mathscr{L}_R[L_{p\alpha}]$ and $\mathscr{L}_R[M_{p\alpha}]$. For a Lambertian surface, the corresponding linearization of BC1, BC2 and BC3 for the Fourier $m = 0$ component gives:

$$\sum_{\alpha=1}^{N} \{\mathscr{L}_R[L_{p\alpha}]X_{-jp\alpha}^{(P)} + \mathscr{L}_R[M_{p\alpha}]\Theta_{p\alpha}X_{-jp\alpha}^{(N)}\} = B_{jp}^{(R1)}, \tag{82}$$

$$\sum_{\alpha=1}^{N} [\{\mathscr{L}_R[L_{r\alpha}]\Theta_{r\alpha}X_{jr\alpha}^{(P)} + \mathscr{L}_R[M_{r\alpha}]X_{jr\alpha}^{(N)}\} - \{\mathscr{L}_R[L_{p\alpha}]X_{jp\alpha}^{(P)} + \mathscr{L}_R[M_{p\alpha}]\Theta_{p\alpha}X_{jp\alpha}^{(N)}\}] = B_{jp}^{(R2)}, \tag{83}$$

$$\sum_{\alpha=1}^{N} \{\mathscr{L}_R[L_{p\alpha}]\Theta_{p\alpha}\Phi_{j\alpha}^{(P)} + \mathscr{L}_R[M_{p\alpha}]\Phi_{j\alpha}^{(N)}\} = B_{jp}^{(R3)}, \tag{84}$$

where $B_{jp}^{(R1)} = 0$ for $p = 1$ and $j = 1,\ldots,N$; $B_{jp}^{(R2)} = 0$ for all $p > K$ and $j = 1 \pm 1,\ldots,\pm N$ and

$$B_{jK}^{(R3)} = R\mu_0 F_\odot \mathrm{e}^{-\tau_{\mathrm{spher}}(\tau_K)} - 2R\sum_{i=1}^{N} w_i\mu_i G_{-iK}|_{\tau_K}. \tag{85}$$

We have used (23a) and (23b) to establish $B_{jp}^{(R3)}$ for $p = K$ and $j = 1, \ldots, N$. Again, we have the same linear system, this time with a new source vector constructed from the right-hand entries. The solution for $\mathscr{L}_R[L_{p\alpha}]$ and $\mathscr{L}_R[M_{p\alpha}]$ follows once again by back-substitution.

Once the linearizations of the integration constants have been found, it is possible to write the linearization of the discrete-ordinate solution anywhere in the atmosphere, and hence we have determined weighting functions at quadrature values and at arbitrary optical depth. In order to complete the weighting function solution for arbitrary stream angles, we now look at the linearization analysis of the post-processing function.

4.6. Linearization analysis of the post-processing function

We return to expressions (24a) and (24b) for the partial layer intensities derived using the source function integration technique. Since $\mathscr{L}_q[\Delta_q] = \Delta_q v_q$ and $\mathscr{L}_q[x] = x v_q$ for x in layer q, we have

$$\mathscr{L}_q[I^+(x,\mu)] = \{\mathscr{L}_q[I_p^+(\mu)] - \delta_{pq} v_q (\Delta_p - x)\mu^{-1} I_p^+(\mu)\} \mathrm{e}^{-(\Delta_p - x)/\mu} + \varepsilon_{pq} \mathscr{L}_q[\Lambda_p^+(x,\mu)], \tag{86a}$$

$$\mathscr{L}_q[I^-(x,\mu)] = \{\mathscr{L}_q[I_{p-1}^-(\mu)] - \delta_{pq} v_q x \mu^{-1} I_{p-1}^-(\mu)\} \mathrm{e}^{-x/\mu} + \varepsilon_{pq} \mathscr{L}_q[\Lambda_p^-(x,\mu)], \tag{86b}$$

where $\delta_{pq} = 1$ for $p = q$ and $\delta_{pq} = 0$ otherwise, and $\varepsilon_{pq} = 1$ for $p \geqslant q$ and $\varepsilon_{pq} = 0$ for $p < q$. The latter condition arises from the fact that the source terms $\Lambda_p^{\pm}(x,\mu)$ have no linearization for $p < q$. Expressions for whole layers can be obtained by setting $x = 0$ in (86a) and $x = \Delta_p$ in (86b).

Recalling the expression (26) for the source function terms, we write

$$\mathscr{L}_q[\Lambda_p^{\pm}(x,\mu)] = \mathscr{L}_q[H_p^{\pm}(x,\mu)]\delta_{pq} + \mathscr{L}_q[D_p^{\pm}(x,\mu)] + \mathscr{L}_q[E_p^{\pm}(x,\mu)]. \tag{87}$$

This is valid for variations in layers $p \leqslant q$. Note that the homogeneous solution contribution $H_p^{\pm}(x,\mu)$ has no variation outside layer q. Finding the linearizations of the three quantities on the right hand side of this equation is a straightforward but lengthy exercise; one proceeds using already-established results from the linearization of the discrete ordinate solution, along with repeated applications of the chain rule. The mathematical details are given in Appendix C.1 for the three right hand side terms in (87) respectively.

As with the intensity calculation, the above results can be used recursively to generate weighting functions at arbitrary optical depth and direction. For whole layer terms we simply set $x = \Delta_p$ or $x = 0$ for layer p. For the upwelling values at point x in layer p, we start with the bottom-of-the atmosphere linearization $\mathscr{L}_q[I^+(\tau_K,\mu)]$ and use the whole-layer expressions repeatedly for layers below p, followed by a single partial-layer application of (86a) in layer p to finish. Care should be taken to distinguish the cases $p = q$, $p < q$ and $p > q$.

5. The LIDORT package

Based on the theory presented in this paper and the preceding one (SKC), the numerical model LIDORT (Linearized Discrete Ordinate Radiative Transfer) has been developed as a general tool

for use in forward model studies connected with atmospheric retrieval. The model can be used in an intensity-only mode (without the linearization options) or additionally to generate simultaneous fields of weighting functions. The first version based on SKC dealt with the satellite application in a plane-parallel atmosphere. The second version has two important extensions to cover the pseudo-spherical treatment of the direct beam attenuation and to generate output for any atmospheric application. The LIDORT V2 package has the following attributes:

1. Multiple scatter treatment of the radiative transfer equation in an inhomogeneous atmosphere, with any number of scatterers. A general treatment for a bi-directionally reflecting surface is available;
2. Generation of upwelling and/or downwelling intensity and weighting function fields for arbitrary viewing geometry and optical depth;
3. Option to perform a plane-parallel calculation or a pseudo-spherical calculation using the average secant approximation. Both methods of particular integral solution (classical and Green's function) are implemented;
4. Weighting functions may be generated with regard to any atmospheric parameter that causes variation in layer extinction coefficient and single-scatter albedo. Options to output weighting functions with respect to albedo and surface blackbody temperature are implemented;
5. Additional output includes mean-value quantities (flux, mean intensity) and their weighting functions, and layer-integrated multiple scatter source terms and associated weighting functions;
6. The delta-M scaling transformation has been incorporated both in the intensity calculation and in the weighting function analysis.

Double precision arithmetic is used throughout LIDORT; the code is written in FORTRAN 77. For the numerical tools, the module ASYMTX from DISORT was used for the homogeneous solution eigenproblem, and LAPACK modules [25] were employed for all linear matrix algebra systems. LIDORT contains a standardized error handling procedure in addition to a number of auxiliary routines for both the reading of input data from files, and the generation of result data to file. As noted already, LIDORT is a pure scattering formalism; there are no databases or climatologies of atmospheric and optical properties in the model. The LIDORT package is called as a subroutine within a user-defined environment; the usage is similar to that for DISORT [6]. The software has been quality controlled and is portable and robust; it can be installed on PCs under the Linux operating system. Memory requirements are modest.

For the average secant parameterization, both methods of particular integral solution (Green's function and substitution) are implemented in the software. Intensity results for the two methods were found to be identical to 9 places of decimals. Computation speeds are similar: the Green's function method is faster for the determination of the discrete ordinate solution, but a little slower for the post-processing step. An off-line intensity-only version of LIDORT has been written to deal with the exponential-sine and exponential-polynomial parameterizations of the direct beam transmittance.

All plane-parallel intensity output was verified using the DISORT model; pseudo-spherical results were validated against the SDISORT code [23]. Table 1 gives a sample of these validations for the test atmosphere described in Section 6.1. Results are for upwelling intensities at TOA for line-of-sight viewing zenith angles as indicated. DISORT comparisons were done for a solar zenith angle of 15°, SDISORT validations with solar angle 82°; in both cases the relative azimuth angle was 60°. The

Table 1
TOA upwelling intensity: LIDORT plane-parallel (PP) and DISORT, LIDORT pseudo-spherical (PS) and SDISORT

Angle (◦)	DISORT	LIDORT PP	SDISORT	LIDORT PS
0.0	8.83804E−02	8.838043E−02	1.74379E−02	1.743787E−02
1.0	8.82865E−02	8.828647E−02	1.74259E−02	1.742588E−02
2.0	8.81990E−02	8.819904E−02	1.74194E−02	1.741939E−02
5.0	8.79799E−02	8.797986E−02	1.74333E−02	1.743328E−02
10.0	8.77839E−02	8.778397E−02	1.75709E−02	1.757091E−02
15.0	8.78271E−02	8.782700E−02	1.78613E−02	1.786122E−02
20.0	8.81004E−02	8.810022E−02	1.83187E−02	1.831864E−02
25.0	8.86090E−02	8.860901E−02	1.89573E−02	1.895727E−02

figures apply to a 60-layer atmosphere with 10 discrete ordinate streams in the half-space for the DISORT validation, and 8 streams for the SDISORT comparison.

All weighting function output may be verified against finite-difference estimates

$$\mathscr{K}_{\mathrm{FD}}(\xi_q) \simeq (I(\xi_q^+) - I(\xi_q^-))/(2\varepsilon_{\mathrm{FD}}), \tag{88}$$

where $I(\xi_q^{\pm})$ are the intensities calculated using perturbed values $\xi_q^{\pm} = \xi_q(1 \pm \varepsilon_{\mathrm{FD}})$ of parameter ξ_q in layer q for an external perturbation $\varepsilon_{\mathrm{FD}}$. For parameters such as volume mixing ratio for which the optical thickness dependence is linear, agreement between analytically-derived results $\mathscr{K}_{\mathrm{LIDORT}}(\xi_q)$ and the finite-difference equivalents $\mathscr{K}_{\mathrm{FD}}(\xi_q)$ can be made very close for small enough $\varepsilon_{\mathrm{FD}}$. For other parameters such as temperature, where the optical property dependence is usually non-linear, the finite-difference result is at best an approximation.

The delta-M scaling transformation [22] is a useful adjunct to any radiative transfer model dealing with multiple scattering. It provides a convenient way of dealing with phase functions which are sharply peaked in the forward scattering direction; the original phase function is replaced by a delta-function forward peak plus a smoother residual which requires a limited number of Legendre phase function moments for its description. The delta-M process essentially involves an initial scaling of the optical depth inputs (single scattering albedo and vertical optical depth) before the RTE is solved. (Slant path optical thickness inputs must also be scaled when the pseudo-spherical treatment is required in the RTE solution). In a model with a simultaneous weighting function capability, it is also necessary to scale the variational inputs $\{u_q, v_q\}$ before the RTE is linearized. Details of the delta-M scaling transformations for LIDORT are presented in Appendix D.

Creating the right inputs for the model is very important, and we will examine this in more detail in the next section when we consider examples in a real atmospheric situation. We enumerate here the main *geophysical* inputs:

1. Layer single scattering albedos ω_{qs} for any number of scatterers, each such albedo normalized to the total layer extinction coefficient. A vertical optical depth grid τ_q, plus layer slant path optical thicknesses κ_{qp} for each layer p traversed by the direct beam in its path to a scatter point at vertical optical depth τ_q.
2. Surface albedo R and an albedo-normalized bi-directional reflection function specified at all stream angles (ordinates and off-quadrature) for sufficient Fourier terms.

3. Layer phase function moment coefficients β_{lqs} for layer q, scatterer s in this layer, and for sufficient Legendre moments l to ensure valid application of the delta-M scaling.
4. Variational input $u_{q\xi s}$ which is the relative differential variation of layer single scattering albedo ω_{qs} with respect to atmospheric parameter ξ. Variational input $v_{q\xi}$ which is the relative differential variation of layer extinction coefficient e_q with respect to atmospheric parameter ξ.

The LIDORT User's Guide has a description of the complete package, and a discussion with examples on the construction of a typical environment for the model and an interface to set up the appropriate optical property inputs. The User's Guide also contains instructions on installation and execution. A test data set has been prepared for release; this is based in part on the example described in detail in below. The LIDORT source code and User's Guide may be downloaded from the SAO web site (http://cfa-www.harvard.edu/pub/lidort/v2).

6. Nadir and zenith examples with the LIDORT model

6.1. Construction of LIDORT inputs for a terrestrial scenario

For the applications considered below in Sections 6.2 and 6.3, we take a terrestrial atmosphere with height 60 km, a vertical height resolution of 1 km, with O_3 volume mixing ratios (VMRs) X_q, temperatures T_q and pressures P_q for a "tropical" standard atmosphere [27], interpolated to the mid-points of each layer. We choose a range of wavelengths in the UV covering the O_3 Hartley–Huggins absorption bands. We take O_3 cross sections $\sigma_q^{O_3}$ (cm^2) for layers q to possess quadratic temperature-dependency. Thus $\sigma_q^{O_3} = \sigma_0 + T_q\sigma_1 + T_q^2\sigma_2$, where T_q is in °C. Coefficients $\sigma_0, \sigma_1, \sigma_2$ are taken from a standard data set [28].

Molecular (Rayleigh) scattering and aerosol scattering are present in all layers. For the wavelength dependence of the Rayleigh scattering cross section σ^{Ray} (cm^2) and the depolarization ratio δ_{Ray}, we use empirical formulae [29] based on data from Bates [30]. The only non-zero phase function moment coefficients are $\beta_0^{Ray} = 1$ and $\beta_2^{Ray} = (1 - \delta_{Ray})/(2 + \delta_{Ray})$. For the aerosol properties, a LOWTRAN model [31] is selected, with maritime-type boundary layer aerosol (visibility 23 km, relative humidity 70%) and background stratospheric and tropospheric optical properties. Aerosol scattering coefficients σ_q^{Aer} and extinction coefficients e_q^{Aer} (in (cm^{-1})) are linearly interpolated to wavelength. For the aerosols we assume Henyey–Greenstein phase functions with asymmetry parameters g taken from the appropriate selection of LOWTRAN aerosol types and interpolated linearly with wavelength (phase function moment coefficients are $\beta_0^{Aer} = 1$, and $\beta_l^{Aer} = g^l$ for $l > 0$). The clear sky total optical thickness for this atmosphere is 1.256 at wavelength 335.4579 nm, with corresponding total Rayleigh scattering optical thickness 0.759, and total ozone absorption optical thickness 0.00707.

We illustrate the construction of LIDORT inputs for this atmosphere. Writing ρ_q for the average air number density (cm^{-3}), e_q for the layer total extinction coefficient, Δ_q the layer optical thickness, and ω_q^{Ray} and ω_q^{Aer} for the layer single scattering albedos, we get:

$$e_q = \rho_q[X_q\sigma_q^{O_3} + \sigma^{Ray}] + e_q^{Aer}, \quad \text{with } \Delta_q = e_q h_q, \tag{89a}$$

$$\omega_q^{Ray} = \rho_q\sigma^{Ray}/e_q \quad \text{and} \quad \omega_q^{Aer} = \sigma^{Aer}/e_q, \tag{89b}$$

where h_q is the layer geometrical thickness (cm). Together with β_l^{Ray} and β_l^{Aer}, these results define the LIDORT model input for the plane-parallel atmosphere in an intensity-only mode. For the pseudo-spherical approximation, we need the slant optical depths κ_{pq} as defined in (32); since the extinctions are known, these layer optical depths can be specified once the slant path distances s_{pq} in (32) have been worked out from a suitable ray-tracing program.

The second step concerns inputs $\{u_q, v_q\}$ for the weighting functions. The definitions are $\mathscr{L}_q[\omega_q] = \xi_q \partial\omega_q/\partial\xi_q = u_q\omega_q$ and $\mathscr{L}_q[e_q] = \xi_q \partial e_q/\partial\xi_q = v_q e_q$. We consider two atmospheric parameters ξ: the volume mixing ratio X_q and the temperature T_q. For $\xi = X_q$, the dependence on X_q is straightforward and we can write

$$u_{\xi q}^{\mathrm{Ray}} = -\rho_q X_q \sigma_q^{\mathrm{O_3}}/e_q, \quad u_{\xi q}^{\mathrm{Aer}} = -\rho_q X_q \sigma_q^{\mathrm{O_3}}/e_q \quad \text{and} \quad v_{\xi q} = +\rho_q X_q \sigma_q^{\mathrm{O_3}}/e_q. \tag{90}$$

For $\xi = T_q$ the dependence is more complex. From the temperature dependence of the cross-sections, we find $\partial\sigma_q^{\mathrm{O_3}}/\partial T_q = \sigma_1 + 2T_q\sigma_2$. Also we have $\partial\rho_q/\partial T_q = -\rho_q/T_q$, since $\rho_q = \rho_{\mathrm{S}}(P_q T_{\mathrm{S}})/(P_{\mathrm{S}} T_q)$ (the S suffix indicates values for a standard atmosphere). Using this information in the definitions gives us

$$u_{\xi q}^{\mathrm{Ray}} = -T_q^{-1} - \mathrm{e}_q^{-1}\partial e_q/\partial T_q, \quad u_{\xi q}^{\mathrm{Aer}} = -\mathrm{e}_q^{-1}\partial e_q/\partial T_q \quad \text{and} \quad v_{\xi q} = +\mathrm{e}_q^{-1}\partial e_q/\partial T_q, \tag{91}$$

where

$$\partial e_q/\partial T_q = -\rho_q T_q^{-1}(X_q\sigma_q^{\mathrm{O_3}} + \sigma_q^{\mathrm{Ray}}) + \rho_q X_q(\sigma_1 + 2T_q\sigma_2). \tag{92}$$

6.2. Intensity and O_3 VMR weighting functions from LIDORT

We look at two nadir viewing situations: (1) the upwelling radiation field at TOA as seen by a nadir-viewing satellite such as GOME, GOME-2 or SCIAMACHY; and (2) the downwelling radiation at the surface as seen by a ground-based instrument measuring sky radiances. In both cases, we assume a Lambertian surface and no surface or atmospheric thermal emission. We show results for a wide range of solar zenith angles, concentrating in particular on the higher values from 65° to 89.5° in order to examine the effect of the pseudo-spherical approximation. Line-of-sight zenith angles will range from 0° to 35°, with azimuth angles as noted. A 10-stream discrete ordinate solution was used in LIDORT, with an accuracy criterion of 0.001 on the convergence of the Fourier azimuth series (this model control is sufficient for a UV scenario with a large Rayleigh scattering component). The examples that follow are indications of the output that the model can generate.

First we compare pseudo-spherical intensities against comparable plane-parallel results. Fig. 3 (top panel) shows the differences between the TOA upwelling intensities calculated using the plane-parallel mode and average secant parameterization to the pseudo-spherical mode. The limitation on the validity of the plane-parallel assumption is clear. A similar picture emerges for downwelling intensities at the bottom of the atmosphere (BOA) (bottom panel). These intensities were calculated at a single wavelength (335.4579 nm) for a number of solar zenith angles as indicated, for a range of line-of-sight angles up to 25° and for a relative azimuth of 60°.

Next we look at the pseudo-spherical approximation in a little more detail. In Fig. 4, we show the effect of neglecting refraction using the average secant parameterization. As noted before, the

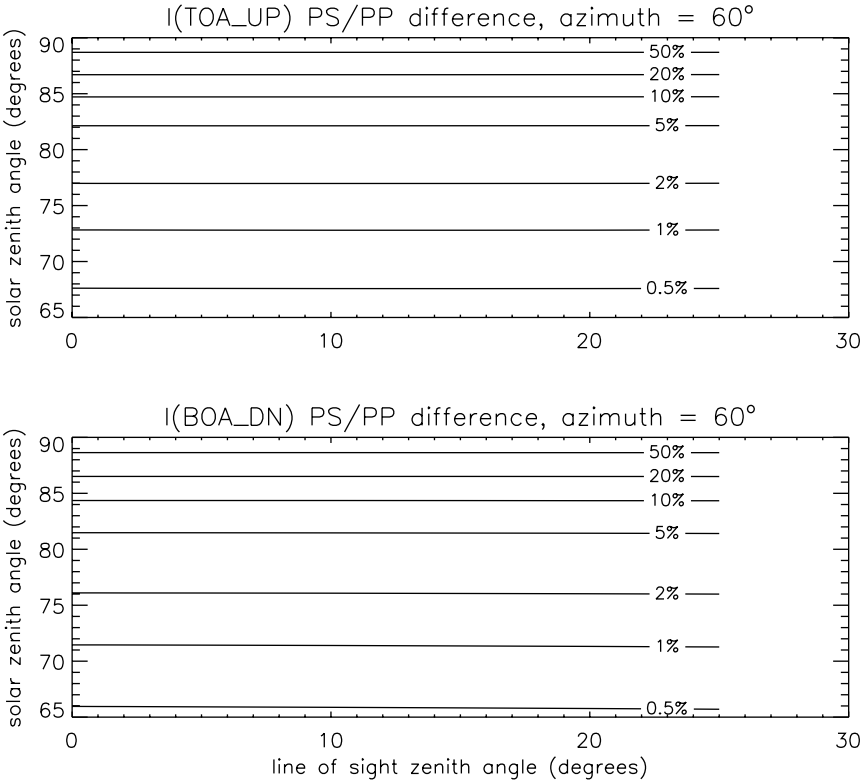

Fig. 3. (Top) TOA upwelling intensities: % difference between pseudo-spherical (average secant) and plane-parallel results for the geometries indicated, albedo 0.3, wavelength 335.4579 nm; (bottom) the same comparison for downwelling intensity at the lower boundary.

inclusion of refraction is really a question of providing properly ray-traced optical depth inputs; the execution of LIDORT itself is not affected by this input choice. All computations were done for the azimuth-independent term (nadir/zenith viewing) and for a number of heights (optical depths) through the atmosphere. The top panel (for the upwelling field) indicates the spread of differences through the atmosphere; the peak around 18 km is clear. The difference is less noticeable for downwelling intensities (lower panel), where the largest effect is close to the surface for the highest solar zenith angles.

The average secant pseudo-spherical parameterization is adequate for clear sky scenarios with a number of optically thin layers. We now examine a scenario where a more accurate parameterization of the direct beam is useful. To the atmosphere described in Section 6.1, we add a highly scattering optically thick particulate in one layer. We take a hypothetical polar stratospheric cloud (PSC) scenario, with a cloud layer of optical thickness 1.0 and single scattering albedo 0.996 between 24 and 25 km. The solar zenith angle is 88°; at this sort of incidence, layers beneath the cloud will be opaque to direct beam illumination and the light is multiply scattered in this part of the atmosphere. Fig. 5 shows upwelling intensity LIDORT results for 3 line-of-sight viewing angles at a relative azimuth of 60°, calculated with the average secant and exponential-polynomial parameterizations

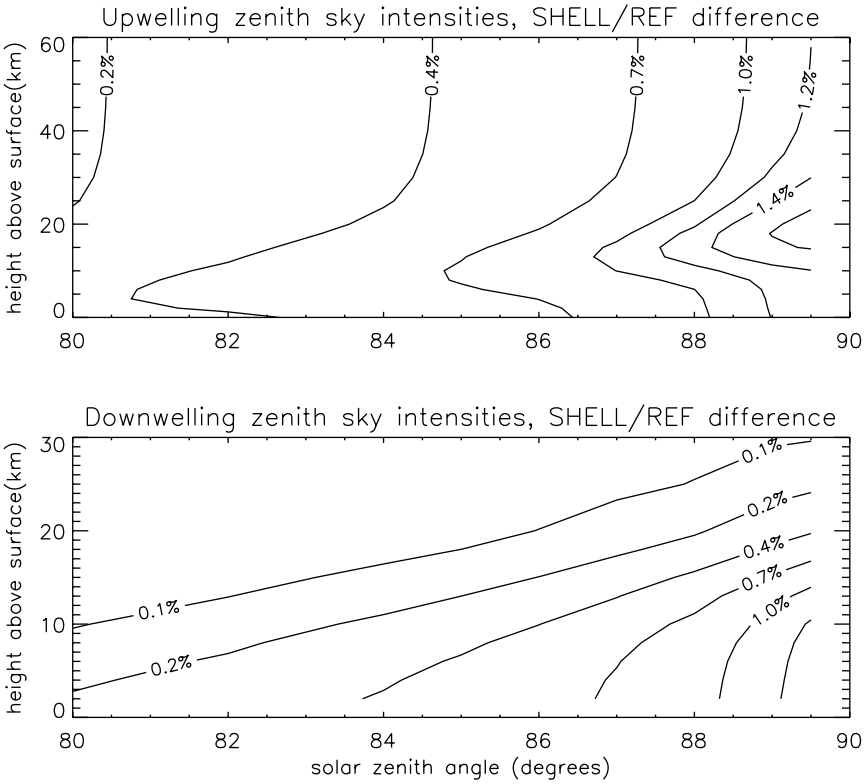

Fig. 4. (Top) Zenith upwelling intensities in the whole atmosphere: a comparison with and without refraction using the pseudo-spherical average secant parameterization. Albedo and wavelength as in Fig. 3; (bottom) similar comparison for zenith downwelling intensities in the lower atmosphere.

of the direct beam attenuation. The latter parameterization required 3 fitted coefficients to ensure an accuracy of 1% in the beam attenuation through the cloud layer. For the viewing geometries considered, errors in the intensity due to the average secant approximation are in the range 2.5–4%. It is clear that for atmospheres with cloud layers, an improved direct beam parameterization will result in significantly better intensity accuracy.

We now look at some weighting function output. Fig. 6 shows the weighting functions with respect to O_3 volume mixing ratio for all levels in the atmosphere, and for a number (10) of wavelengths in the Hartley–Huggins range of ozone absorption. Results have been normalized to the peak values; a pseudo-spherical calculation was performed for albedo 0.3, for two solar zenith angles 35° and 82°, line of sight 15° and relative azimuth 0°. Below 300 nm, peak values occur at heights that increase with lower wavelengths. It is this well-known differential scattering height behavior that underpins the BUV technique for O_3 profile retrieval in the stratosphere [32]. Note also the increasing tropospheric sensitivity for the longer wavelengths; this sensitivity tends to disappear with increasing solar zenith angle.

Fig. 7 shows nadir-view O_3 VMR weighting functions at one wavelength (335.4579 nm), calculated in the average secant pseudo-spherical and plane-parallel approximations for a number of solar zenith

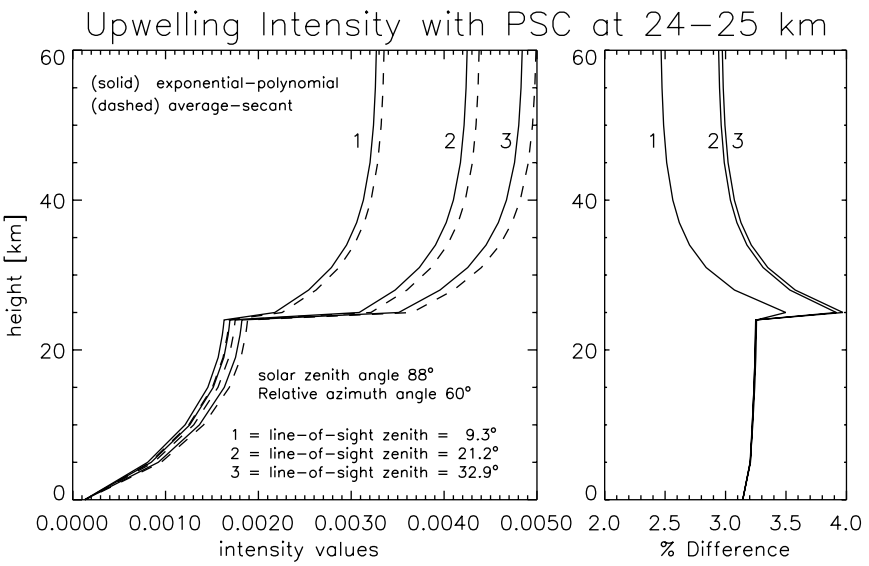

Fig. 5. Upwelling intensities in the atmosphere using the average secant and exponential-polynomial pseudo-spherical parameterizations: a comparison. Albedo and wavelength as in Fig. 3; geometries as indicated.

angles. The top panel shows results for the satellite application (TOA upwelling) at four selected solar zenith angles. There is a significant loss of tropospheric sensitivity for higher solar zenith angles. Note also the spurious upward drift of the peak sensitivity for the plane-parallel results. The lower panel illustrates in more detail the differences in these results.

6.3. LIDORT model simulations for wide off-nadir satellite viewing

Under normal viewing conditions, GOME-2 has a swath width of 1920 km; at the extremes, the line-of-sight at the satellite is $\simeq 48^\circ$ from the nadir (this translates to a zenith angle of $\simeq 55.3^\circ$ at the top of an atmosphere of height 100 km). The swath for the OMI instrument is even larger ($\simeq 2600$ km), the off-nadir line-of-sight angle at the satellite being 57° at the swath ends. Wide-angle views are also a feature of the GOME and SCIAMACHY instruments operating in special polar-viewing modes [9]. As noted in the Introduction, the regular pseudo-spherical model treats all scatter events along the zenith AC in Fig. 1 (the solar zenith angle is always θ_A); the solar path to the point of scatter is attenuated in a curved atmosphere. In the enhanced pseudo-spherical approach, we consider precise calculations of the single scatter at all points P_n along AB, treating both solar beam and line-of-sight attenuation for the curved atmosphere. All multiple scatter contributions to the upwelling intensity I_B are computed from regular LIDORT computations done for points along AB. We adopt the source function integration method to compute I_B.

Referring to Fig. 1, consider points P_n and P_{n-1} at the lower boundaries of layers n and $n-1$ respectively. Using an integration of the RTE along the segment P_nP_{n-1}, we can write:

$$I_{n-1} = I_n\Theta_n + \Lambda_n^{(SS)} + \Lambda_n^{(MS)}, \tag{93}$$

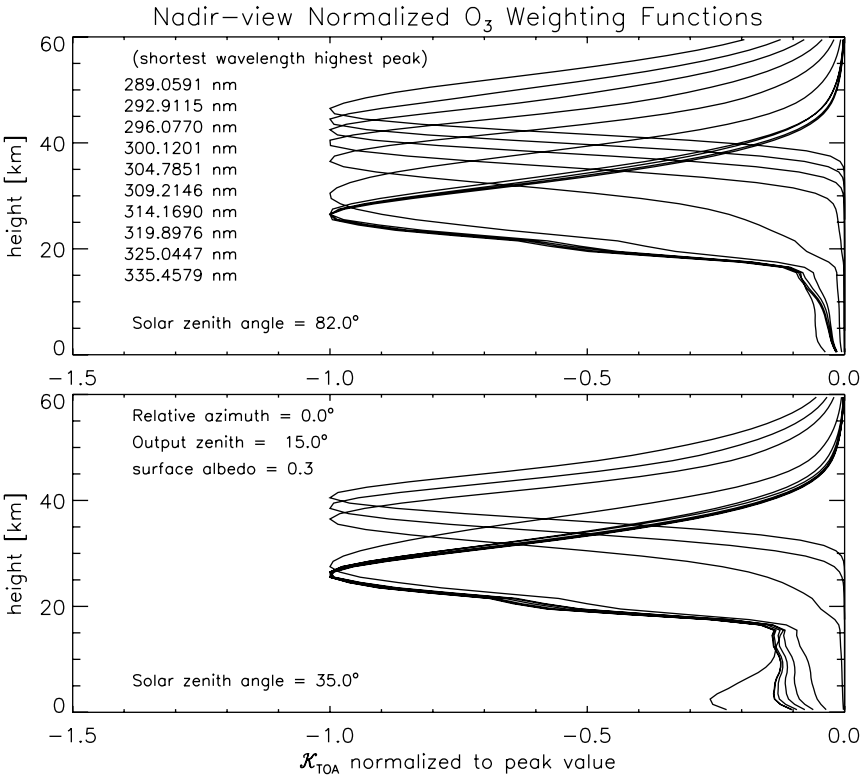

Fig. 6. TOA upwelling O_3 VMR weighting functions for a number of wavelengths as indicated. Output is normalized to the peak values.

where Θ_n is the line-of-sight transmittance along the segment, $\Lambda_n^{(SS)}$ is the layer-integrated single scatter contribution to the upwelling radiance, and $\Lambda_n^{(MS)}$ is the layer-integrated upwelling multiple scatter contribution. For a curved atmosphere with appropriate viewing geometry along the segment, Θ_n and $\Lambda_n^{(SS)}$ are evaluated accurately in a separate calculation for the single scatter. $\Lambda_n^{(MS)}$ is simply replaced by the upwelling whole layer multiple scatter contribution derived in Eq. (29) from the LIDORT model. Since viewing geometries vary along AB, separate LIDORT calculations should be done for each geometry $\{\theta_n, \alpha_n, \phi_n\}$ at P_n (where ϕ_n is the relative azimuth angle).

The recursion (93) starts with the upwelling intensity I_A at the lower boundary at position A, and finishes with I_B, the upwelling intensity at B. I_A is returned from a LIDORT calculation with the appropriate geometry at A. Between A and B, one can reduce the number of intermediate multiple scatter calculations by calling LIDORT for a small subset of points along AB (to include the first and last points P_1 and A), and then interpolating the multiple scatter source term output against the cosine of the solar zenith angle along AB. (Remember that a single LIDORT call can return layer-integrated multiple scatter terms for *all* layers in the atmosphere). Any error induced by this interpolation will be very much smaller than the basic enhancement itself. Note also that the corrected single scatter computation uses the phase function directly without the truncation implicit in the discrete ordinate treatment. A similar approach us-

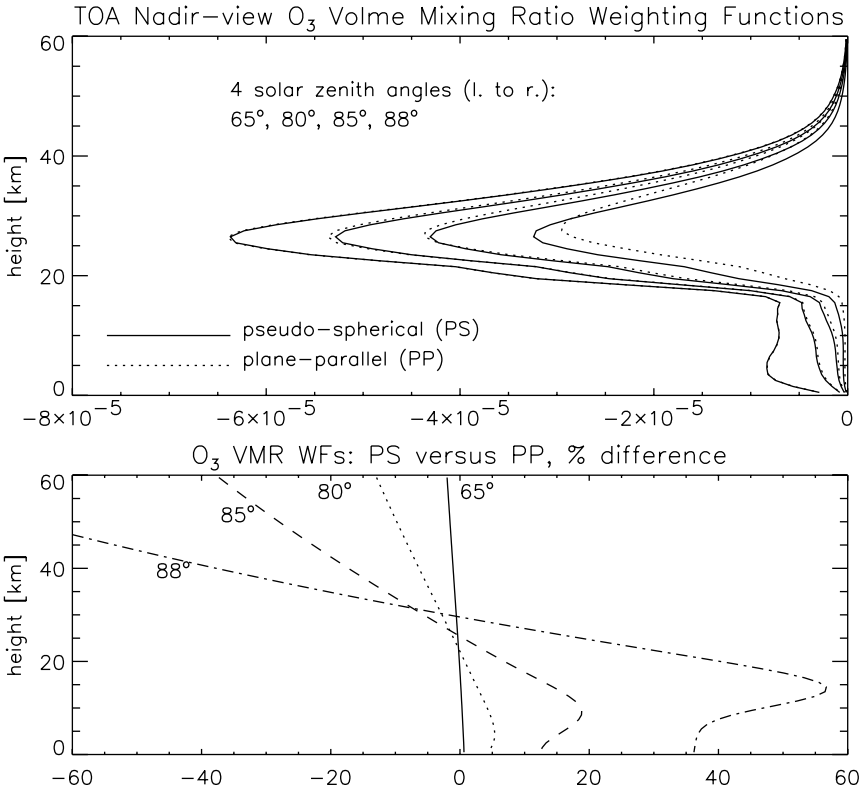

Fig. 7. (Top panel) TOA upwelling O_3 weighting functions in the nadir direction for 4 solar zenith angles, wavelength 335.4579 nm, albedo 0.3; (lower panel) corresponding percentage differences.

ing multiple-scatter source terms has been developed for the pseudo-spherical GOMETRAN finite-difference model [33].

In a non-refractive atmosphere, the scattering angle is a constant for all points on the path AB. Fig. 1 illustrates the forward scatter situation; for the backward (antisolar) scenario, the scatter angle will be quite different. We can thus expect some additional asymmetry between the forward and backward scatter cases. Also, in the forward scatter scenario the solar zenith angle at A is less than the value at B; for the backward scatter case, the reverse is true (the difference is about $\mp 1.5^\circ$ for a TOA line-of-sight zenith of 60° for the solar/antisolar positions). This variation in solar zenith angle is an additional source of asymmetry, both in the single scatter calculation and in the multiple scatter source terms.

Fig. 8 shows the differences between regular pseudo-spherical LIDORT output and improved estimates of intensity using the multiple-scatter layer-integrated source term output from LIDORT and the corrected single scatter calculation. Intensity results were performed for 0° (solar) and 180° (antisolar) azimuth angles, for a solar zenith angle of 85° and for line-of-sight angles from 0 to 70°. The results were performed at five different wavelengths in the UV for the atmosphere outlined in Section 6.1 but without aerosols (Rayleigh scattering alone) and with a surface albedo of 0.1. The results mirror closely those found in [33]. In general the absolute magnitude of the correction

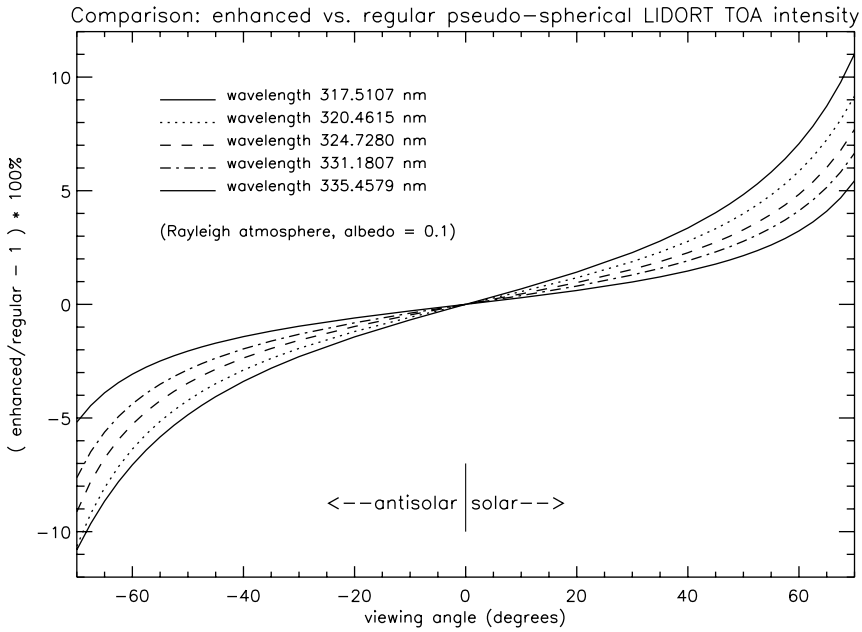

Fig. 8. Comparison of TOA upwelling intensities from regular and enhanced pseudo-spherical model output, for 0° (solar) and 180° (antisolar) azimuth angles, solar zenith angle 85°. Rayleigh atmosphere, albedo 0.1. 5 wavelengths as indicated.

is greater for the antisolar scenarios. It is immediately clear that this correction is essential for the wide-angle viewing geometries of GOME-2 and OMI; differences for viewing zenith angles in excess of 50° vary from 3% to 8%.

The situation for weighting functions is also straightforward. With respect to an atmospheric parameter ξ_q in layer q, we may apply the linearization operator $\mathscr{L}_q$ to the recursion (93):

$$\mathscr{L}_q[I_{n-1}] = \mathscr{L}_q[I_n]\Theta_n + I_n\delta_{qn}\mathscr{L}_n[\Theta_n] + \mathscr{L}_q[\Lambda_n^{(\mathrm{SS})}] + \mathscr{L}_q[\Lambda_n^{(\mathrm{MS})+}]. \tag{94}$$

Again, $\mathscr{L}_n[\Theta_n]$ and $\mathscr{L}_q[\Lambda_n^{(\mathrm{SS})}]$ may be evaluated directly for a curved atmosphere in a dedicated single scatter calculation. Assuming $\Lambda_n^{(\mathrm{MS})+}$ to be approximated by the pseudo-spherical LIDORT value, then its linearization $\mathscr{L}_q[\Lambda_n^{(\mathrm{MS})+}]$ can also be taken straight from LIDORT output. The linearized recursion starts with $\mathscr{L}_q[I_\mathrm{A}]$ which is returned from the LIDORT calculation at A, and finishes with the weighting function at the top of the atmosphere B.

Fig. 9 shows differences in ozone VMR weighting functions for a solar zenith angle of 85°, a viewing zenith angle of 55° (this is a typical value for GOME-2 at the swath limits), and for the solar and anti-solar positions. Calculations were done for the same atmosphere and wavelengths as used in Fig. 8. The asymmetry between forward and backward scatter weighting function differences is more marked, with a broad bias apparent for the lowest wavelength (greatest sensitivity). It is again clear that the correction will be essential for retrievals of ozone profiles from GOME-2 and OMI.

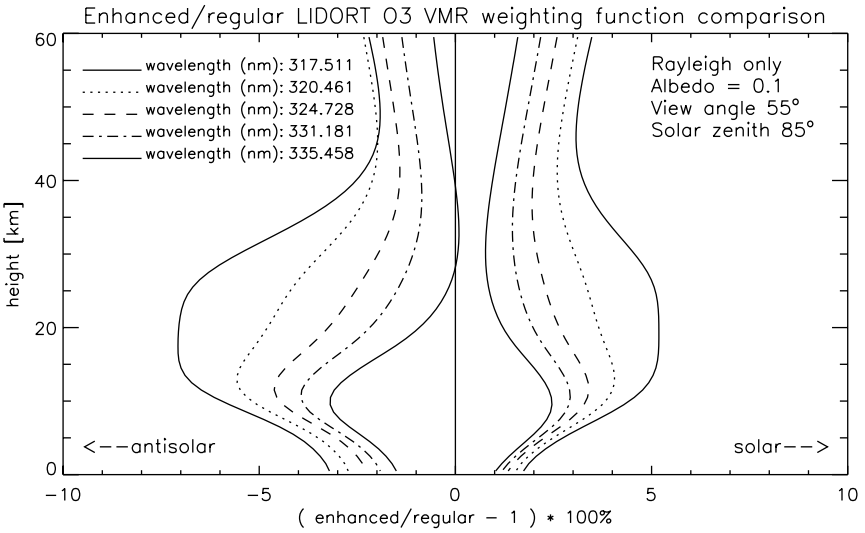

Fig. 9. Comparison of TOA upwelling ozone VMR weighting functions from regular and enhanced pseudo-spherical model output for solar zenith angle 85°, viewing zenith angle 55° and for the solar and anti-solar positions. Atmosphere and wavelengths as in Fig. 8.

7. Concluding remarks

In this paper we have described an extension of the discrete ordinate solution of the radiative transfer equation in a multiply scattering multi-layer atmosphere to the simultaneous calculation of analytically accurate weighting function fields. A pseudo-spherical treatment of the direct beam transmittance enables the backscatter fields to be obtained for a range of solar zenith angles up to 90°. Examples of intensity and weighting function output using the numerical model LIDORT were presented for a number of nadir and zenith viewing earthshine backscatter applications in the UV part of the spectrum.

The GOME, SCIAMACHY and GOME-2 instruments have the ability to measure earthshine spectra in two directions of polarization; intensity measurements are polarization-corrected before use in retrieval algorithms. Vector radiative transfer studies in and around the O_2 A band have shown that the polarization correction is critically important for certain GOME retrievals [34]. Comparisons between scalar (intensity) and polarized vector RT models indicate that the scalar assumption can lead to significant sources of error in the simulation of backscatter intensity [35]. Feasibility studies have shown the value of polarization measurements for the retrieval of aerosol properties (see for example [36]). Polarized light measurements from the POLDER instrument have been used to separate aerosol and surface contributions to earthshine reflectance [37]. This instrument was flown in space on ADEOS-1 (1996–1997) and a second POLDER device will be on board ADEOS-2 scheduled for launch in 2001.

Although there are a number of vector RT models in existence, they all calculate the Stokes vector alone; weighting functions must be estimated by finite differencing. Most retrieval studies using vector RT models have used phase-space diagrams and look-up tables. Vectorized discrete ordinate models have been written for a plane-parallel medium [38,39], but the pseudo-spherical

treatment has not been included. A third version of LIDORT will address these issues, namely the development of a linearization analysis of a vectorized model for the generation of weighting functions, and the use of a consistent pseudo-spherical vector RT treatment.

Acknowledgements

This work was supported in part by a contract from the Deutsches Forschungszentrum für Luft und Raumfahrt, contract number 332/60570480 (SCIAMACHY Data Processor Development), in part from an Ozone SAF Visiting Scientist Grant (P-4799-2-00) at KNMI (Royal Dutch Meteorological Institute), and in part with internal funding from the Smithsonian Astrophysical Observatory. The author would like to thank Piet Stammes for valuable feedback on the manuscript, Hennie Kelder for advice and support, and especially Roeland van Oss for many fruitful discussions regarding this work. Contributions from Thomas Kurosu, Werner Thomas and Knut Stamnes are also gratefully acknowledged.

Appendix A. Green's function optical depth multipliers

We derive Green's function optical depth multipliers (45) for the exponential-sine and exponential-polynomial pseudo-spherical parameterizations. We can define

$$C_\alpha^\pm(x) = \hat{T} \sum_{n=0}^{N^*} c_n K_{n\alpha}^\pm(x) \tag{A.1}$$

by analogy with the coefficient expansions (34a) and (34b), with $c_0 = 1$ for both parameterizations, and $\hat{T}K_{0\alpha}^\pm(x)$ the average secant results already noted in (46).

For the exponential-sine parameterization, the functions $K_{n\alpha}^\pm(x)$ for $n > 0$ are:

$$K_{n\alpha}^-(x) = \mathrm{e}^{-xk_\alpha} \mathscr{S}_n(f_\alpha^-, x), \tag{A.2a}$$

$$K_{n\alpha}^+(x) = \mathrm{e}^{+xk_\alpha} [\mathscr{S}_n(f_\alpha^+, \Delta) - \mathscr{S}_n(f_\alpha^+, x)] \tag{A.2b}$$

with the definition

$$\mathscr{S}_n(\beta, x) \equiv \int_0^x \mathrm{e}^{-y\beta} \sin(\phi_n y)\, \mathrm{d}y = \frac{\phi_n(1 - \mathrm{e}^{-x\beta}\cos(\phi_n x)) - \beta \mathrm{e}^{-x\beta}\sin(\phi_n x)}{\beta^2 + \phi_n^2}. \tag{A.3}$$

Here, $f_\alpha^\pm = \lambda \pm k_\alpha$ and $\phi_n = \pi n/\Delta$.

For the exponential-polynomial parameterization, the functions $K_{n\alpha}^\pm(x)$ for $n > 0$ are:

$$K_{n\alpha}^-(x) = \mathrm{e}^{-xk_\alpha} \{\Delta \mathscr{Q}_n(f_\alpha^-, x) - \mathscr{Q}_{n+1}(f_\alpha^-, x)\}, \tag{A.4a}$$

$$K_{n\alpha}^+(x) = \mathrm{e}^{+xk_\alpha} \{[\Delta \mathscr{Q}_n(f_\alpha^+, \Delta) - \mathscr{Q}_{n+1}(f_\alpha^+, \Delta)] - [\mathscr{Q}_n(f_\alpha^+, x) - \mathscr{Q}_{n+1}(f_\alpha^+, x)]\} \tag{A.4b}$$

with definitions

$$\mathscr{Q}_n(\beta,x) \equiv \int_0^x \mathrm{e}^{-y\beta} y^n \,\mathrm{d}y, \tag{A.5}$$

$$\beta\mathscr{Q}_n(\beta,x) = n\mathscr{Q}_{n-1}(\beta,x) - x^n\mathrm{e}^{-x\beta} \quad \text{for } n>0 \quad \text{and} \quad \mathscr{Q}_0(\beta,x) = \frac{1-\mathrm{e}^{-x\beta}}{\beta}. \tag{A.6}$$

Appendix B. Integrated source term contributions in the post-processing function

In this appendix, we establish the integrated source term contributions that appear in (26). The appendix is divided into four parts, dealing first with the homogeneous contribution, then the single scatter contribution, followed by the two particular integral contributions evaluated for the classical and Green's function solution methods.

B.1. Homogeneous integrated solution source term contribution

We first look at the contribution $H^{\pm}(x,\mu)$ to the source function terms in (26). This may be written

$$H^{\pm}(x,\mu) = \sum_{\alpha=1}^{N} \{L_\alpha X_\alpha^{(P)}(\mu)\mathscr{H}_\alpha^{\pm+}(x,\mu) + M_\alpha X_\alpha^{(N)}(\mu)\mathscr{H}_\alpha^{\pm-}(x,\mu)\}, \tag{B.1}$$

where the two functions

$$X_\alpha^{(P)}(\mu) = \frac{\omega}{2}\sum_{l=m}^{2N-1}\beta_l P_m^l(\mu)\sum_{j=1}^{N} P_m^l(-\mu_j)w_j X_{j\alpha}^{(P)}, \tag{B.2}$$

$$X_\alpha^{(N)}(\mu) = \frac{\omega}{2}\sum_{l=m}^{2N-1}\beta_l P_m^l(\mu)\sum_{j=1}^{N} P_m^l(+\mu_j)w_j X_{j\alpha}^{(N)} \tag{B.3}$$

can be thought of as the solution vectors $\mathbf{X}_\alpha^{(P)}$ and $\mathbf{X}_\alpha^{(N)}$ defined at off-quadrature directions μ. The sum over j indicates that the discrete-ordinate solutions have been used in the source function derivations. The *integrated homogeneous multipliers* $\mathscr{H}_\alpha^{\pm\pm}(x,\mu)$ arise from the optical depth integrations implicit in the source function derivation. These are straightforward exponential integrals, and the results are

$$\mathscr{H}_\alpha^{++}(x,\mu) = \frac{\mathrm{e}^{-xk_\alpha} - \mathrm{e}^{-\Delta k_\alpha}\mathrm{e}^{-(\Delta-x)/\mu}}{1+\mu k_\alpha} \tag{B.4}$$

$$\mathscr{H}_\alpha^{+-}(x,\mu) = \frac{\mathrm{e}^{-(\Delta-x)k_\alpha} - \mathrm{e}^{-(\Delta-x)/\mu}}{1-\mu k_\alpha} \tag{B.5}$$

for the upwelling source function terms, and

$$\mathscr{H}_\alpha^{-+}(x,\mu) = \frac{\mathrm{e}^{-xk_\alpha} - \mathrm{e}^{-x/\mu}}{1-\mu k_\alpha}, \tag{B.6}$$

$$\mathscr{H}_\alpha^{--}(x,\mu) = \frac{\mathrm{e}^{-(\Delta-x)k_\alpha} - \mathrm{e}^{-\Delta k_\alpha}\mathrm{e}^{-x/\mu}}{1+\mu k_\alpha}, \tag{B.7}$$

for the downwelling terms. These results have appeared a number of times in the literature (see for example [20]). To evaluate whole layer source terms we set $x=0$ in (B.4) and (B.5) for upwelling contributions, and $x=\Delta$ in (B.6) and (B.7) for the downwelling terms. The whole layer multipliers are

$$\mathscr{H}_\alpha^{++}(0,\mu) = \mathscr{H}_\alpha^{--}(\Delta,\mu) = \frac{1-\mathrm{e}^{-\Delta k_\alpha}\mathrm{e}^{-\Delta/\mu}}{1+\mu k_\alpha}, \tag{B.8}$$

$$\mathscr{H}_\alpha^{+-}(0,\mu) = \mathscr{H}_\alpha^{-+}(\Delta,\mu) = \frac{\mathrm{e}^{-\Delta k_\alpha} - \mathrm{e}^{-\Delta/\mu}}{1-\mu k_\alpha}. \tag{B.9}$$

B.2. Primary scatter integrated source term contribution

Next we look at single scatter contributions to the integrated source terms. These are

$$E^{\pm}(x,\mu) = Q^{\pm}(\mu)\mathscr{E}^{\pm}(x,\mu), \tag{B.10}$$

where

$$Q^{\pm}(\mu) = \frac{F_\odot}{2}(2-\delta_{m0})\Pi^m(\mu,-\mu_0) \tag{B.11}$$

and the *single scatter multipliers* $\mathscr{E}_\alpha^{\pm}(x,\mu)$ are

$$\mathscr{E}^{+}(x,\mu) = \frac{\mathrm{e}^{x/\mu}}{\mu}\int_x^\Delta T(y)\mathrm{e}^{-y/\mu}\,\mathrm{d}y \quad \text{and} \quad \mathscr{E}^{-}(x,\mu) = \frac{\mathrm{e}^{-x/\mu}}{\mu}\int_0^x T(y)\mathrm{e}^{y/\mu}\,\mathrm{d}y, \tag{B.12}$$

where $T(y)$ is the direct beam transmittance. These results (B.12) are valid for all parameterizations of the direct beam attenuation; furthermore, they are independent of the Fourier index m in (B.11), so only need evaluation once. The integrations are straightforward for the average secant parameterization $T(y) = \hat{T}\exp(-y\lambda)$:

$$\mathscr{E}^{+}(x,\mu) = \hat{T}\frac{\mathrm{e}^{-x\lambda} - \mathrm{e}^{-\Delta\lambda}\mathrm{e}^{-(\Delta-x)/\mu}}{1+\mu\lambda}, \tag{B.13}$$

$$\mathscr{E}^{-}(x,\mu) = -\hat{T}\frac{\mathrm{e}^{-x\lambda} - \mathrm{e}^{-x/\mu}}{1-\mu\lambda}. \tag{B.14}$$

The plane-parallel result may be obtained by setting $\lambda = \mu_0^{-1}$. Note also that l'Hopital's rule should be used in (B.14) when λ is close to μ^{-1}; the limiting value is:

$$\lim_{\mu\to\lambda}\mathscr{E}^{-}(x,\mu) = -\hat{T}x\lambda\mathrm{e}^{-x\lambda}. \tag{B.15}$$

Whole layer source term contributions are obtained by setting $x=0$ in (B.13) (upwelling), and $x=\Delta$ in (B.14) (downwelling).

For the other pseudo-spherical parameterizations we have some additional terms corresponding to the series expansions used in these approximations. We may write

$$\mathscr{E}^{\pm}(x,\mu) = \mathscr{E}^{\pm}_{\mathrm{AS}}(x,\mu) + \frac{\hat{T}}{\mu}\sum_{n=1}^{N^*} c_n W_n^{\pm}(x,\mu), \tag{B.16}$$

where $\mathscr{E}^{\pm}_{\mathrm{AS}}(x,\mu)$ are the average secant multipliers from (B.13) and (B.14), and for $n>0$,

$$\begin{aligned} W_n^{+}(x,\mu) &= \mathrm{e}^{x/\mu}\int_x^{\Delta} \mathrm{e}^{-y(\lambda+\mu^{-1})}\sin\left(\frac{\pi n y}{\Delta}\right)\mathrm{d}y,\\ W_n^{-}(x,\mu) &= \mathrm{e}^{-x/\mu}\int_0^{x} \mathrm{e}^{-y(\lambda-\mu^{-1})}\sin\left(\frac{\pi n y}{\Delta}\right)\mathrm{d}y \end{aligned} \tag{B.17}$$

for the exponential-sine parameterization, and

$$\begin{aligned} W_n^{+}(x,\mu) &= \mathrm{e}^{x/\mu}\int_x^{\Delta} \mathrm{e}^{-y(\lambda+\mu^{-1})}y^n(\Delta-y)\,\mathrm{d}y,\\ W_n^{-}(x,\mu) &= \mathrm{e}^{-x/\mu}\int_0^{x} \mathrm{e}^{-y(\lambda-\mu^{-1})}y^n(\Delta-y)\,\mathrm{d}y \end{aligned} \tag{B.18}$$

for the exponential-polynomial parameterization. In both cases, the integrals are straightforward and mirror similar calculations in Appendix A.

B.3. Classical particular solution integral source term contributions

We first look at the contributions $D^{\pm}(x,\mu)$ to the source function terms in (26) from the classical form of the particular integral. We do this for the average secant form $G_j(x) = F_j T(x)$, where $T(x) = \hat{T}\exp(-x\lambda)$ and the vector $\mathbf{F}$ was determined in Section 3.3. The results are

$$D^{\pm}(x,\mu) = F^{\pm}(\mu)\mathscr{D}^{\pm}(x,\mu), \tag{B.19}$$

where

$$F^{\pm}(\mu) = \frac{\omega}{2}\sum_{l=m}^{2N-1}\beta_l P_m^l(\mu)\sum_{j=1}^{N} P_m^l(\mp\mu_j)w_j F_j^{\pm} \tag{B.20}$$

can be thought of as the particular solution vector $\mathbf{F}$ defined at off-quadrature streams μ. Since the particular solution has the same optical depth dependence as the single scatter term in the previous section, the *integrated classical solution multipliers* $\mathscr{D}^{\pm}(x,\mu)$ are

$$\mathscr{D}^{\pm}(x,\mu) = \mathscr{E}^{\pm}_{\mathrm{AS}}(x,\mu) \tag{B.21}$$

as defined by results (B.13) and (B.14) for the average secant approximation. One can also use the results in Eqs. (B.16)–(B.18) for the other parameterizations. This would require additional functions such as (B.20) to be defined for each term in the coefficient expansion beyond the average secant.

B.4. Green's function integral source term contributions

Since the Green's function particular integral is also an expansion in terms of homogeneous solution vectors, we would expect the analysis to be similar to that above in Appendix B.1. Recalling the particular integral definitions from Section 3.3, we may write

$$D^{\pm}(x,\mu) = \sum_{\alpha=1}^{N} \{a_\alpha X_\alpha^{(P)}(\mu)\mathscr{D}_\alpha^{\pm+}(x,\mu) + b_\alpha X_\alpha^{(N)}(\mu)\mathscr{D}_\alpha^{\pm-}(x,\mu)\} \tag{B.22}$$

where $X_\alpha^{(P)}(\mu)$ and $X_\alpha^{(N)}(\mu)$ have been defined in (B.2) and (B.3) respectively, with a_α and b_α given by (43).

The *integrated Green's function multipliers* $\mathscr{D}^{\pm\pm}(x,\mu)$ again arise from the optical depth integrations implicit in the source function derivation. They are

$$\mathscr{D}_\alpha^{+\pm}(x,\mu) = \frac{\mathrm{e}^{x/\mu}}{\mu} \int_x^{\Delta} C_\alpha^{\pm}(y)\mathrm{e}^{-y/\mu}\,\mathrm{d}y, \tag{B.23a}$$

$$\mathscr{D}_\alpha^{-\pm}(x,\mu) = \frac{\mathrm{e}^{-x/\mu}}{\mu} \int_0^{x} C_\alpha^{\pm}(y)\mathrm{e}^{+y/\mu}\,\mathrm{d}y, \tag{B.23b}$$

for the upwelling and downwelling contributions respectively. For the average secant (and by default, the plane-parallel) parameterizations, explicit expressions for $C_\alpha^{\pm}(y)$ were written down in (46). Using these results, one can carry out the integrations to give

$$\mathscr{D}_\alpha^{+\pm}(x,\mu) = \frac{\hat{T}\mathrm{e}^{-\Delta\lambda}\mathscr{H}_\alpha^{+\pm}(x,\mu) \pm \mathscr{E}^{+}(x,\mu)}{\lambda \pm k_\alpha}, \tag{B.24a}$$

$$\mathscr{D}_\alpha^{-\pm}(x,\mu) = \frac{\hat{T}\mathrm{e}^{-\Delta\lambda}\mathscr{H}_\alpha^{-\pm}(x,\mu) \pm \mathscr{E}^{-}(x,\mu)}{\lambda \pm k_\alpha}, \tag{B.24b}$$

for upwelling and downwelling multipliers respectively. The quantities $\mathscr{H}_\alpha^{\pm\pm}$ have been determined above in Eqs. (B.4)–(B.7), while $\mathscr{E}^{\pm}$ have been determined for the average secant case in (B.13) and (B.14). Expressions (B.24a) and (B.24b) are convenient for computation; it is obviously possible to write out the full results in terms of many transmittance factors.

For the exponential-sine and exponential-polynomial parameterizations, we can substitute the results of Appendix A for $C_\alpha^{\pm}(y)$ in (B.23a) and (B.23b). All integrals are again straightforward and we summarize the results for the exponential-polynomial parameterization. For the upwelling multipliers, the results are:

$$\mathscr{D}_\alpha^{+\mp}(x,\mu) = \frac{\hat{T}}{\mu}\,\mathrm{e}^{+x/\mu} \sum_{n=0}^{N^*} c_n K_{n\alpha}^{+\mp}(x,\mu), \tag{B.25}$$

where $c_0 = 1$, and the first term in the series duplicates the average secant result (B.24a). For $n > 0$ the K-functions are:

$$K_{n\alpha}^{+\mp}(x,\mu) = \mathscr{C}_{n\alpha}^{\mp}(x,\mu) \mp \Delta\mathscr{R}_n(f_\alpha^{\mp}, g_\alpha^{\pm}, x) \pm \mathscr{R}_{n+1}(f_\alpha^{\mp}, g_\alpha^{\pm}, x) \tag{B.26}$$

with the function $\mathscr{R}$ defined by the recurrence relation

$$\beta\mathscr{R}_{n+1}(\beta,\gamma,x) = n\mathscr{R}_{n-1}(\beta,\gamma,x) - \mathscr{Q}_n(\beta+\gamma,x) \tag{B.27}$$

for general inputs β and γ. The function $\mathscr{Q}_n(\beta,x)$ was defined in (A.5). The particular arguments are $f_\alpha^\pm = \lambda \pm k_\alpha$ and $g_\alpha^\pm = \mu^{-1} \pm k_\alpha$. We also have

$$\mathscr{C}_{n\alpha}^-(x,\mu) = \Delta\mathscr{R}_n(f_\alpha^-, g_\alpha^+, \Delta) - \mathscr{R}_{n+1}(f_\alpha^-, g_\alpha^+, \Delta), \tag{B.28}$$

$$\mathscr{C}_{n\alpha}^+(x,\mu) = \mathscr{J}_{n\alpha}(\mu)[\mathscr{Q}_0(g_\alpha^-, \Delta) - \mathscr{Q}_0(g_\alpha^-, x)] - \Delta\mathscr{R}_n(f_\alpha^+, g_\alpha^-, \Delta) + \mathscr{R}_{n+1}(f_\alpha^+, g_\alpha^-, \Delta), \tag{B.29}$$

$$\mathscr{J}_{n\alpha}(f_\alpha^+) = \Delta\mathscr{Q}_n(f_\alpha^+, \Delta) - \mathscr{Q}_{n+1}(f_\alpha^+, \Delta). \tag{B.30}$$

For the downwelling multipliers, one finds similar results:

$$\mathscr{D}_\alpha^{-\pm}(x,\mu) = \frac{\hat{T}}{\mu}\,\mathrm{e}^{-x/\mu} \sum_{n=0}^{N^*} c_n K_{n\alpha}^{-\pm}(x,\mu), \tag{B.31}$$

where $c_0 = 1$, and the first term in the series duplicates the average secant result (B.24b). For $n > 0$ the K-functions are:

$$K_{n\alpha}^{-\pm}(x,\mu) = \mathscr{C}_{n\alpha}^{\pm}(x,\mu) \pm \Delta\mathscr{R}_n(f_\alpha^{\mp}, -g_\alpha^{\mp}, x) \mp \mathscr{R}_{n+1}(f_\alpha^{\mp}, -g_\alpha^{\mp}, x) \tag{B.32}$$

with the function $\mathscr{R}$ defined in (B.27), and $f_\alpha^\pm$ and $g_\alpha^\pm$ as before. We also have

$$\mathscr{C}_{n\alpha}^-(x,\mu) = 0, \tag{B.33}$$

$$\mathscr{C}_{n\alpha}^+(x,\mu) = \mathscr{J}_{n\alpha}(f_\alpha^+)\mathscr{Q}_0(-g_\alpha^+, x), \tag{B.34}$$

where $\mathscr{J}_{n\alpha}(f_\alpha^+)$ was given in (B.30).

Appendix C. Linearization analysis of the post-processing source terms

We wish to apply the linearization operator $\mathscr{L}$ to each of the source term contributions that appear in the post-processing result (26). The procedure is based on linearization results already obtained for the discrete ordinate solutions in all layers and the linearizations of the boundary value constants, and application of the chain rule of differentiation. The algebraic manipulations are fairly extensive but quite straightforward, illustrating once again that the determination of partial derivatives of the complete discrete ordinate intensity field can be done in an entirely analytic fashion. We follow the same sequence as in the previous appendix. Linearizations for the particular integrals and the single scatter terms are confined to the average secant parameterization of the pseudo-spherical treatment.

C.1. Linearization of the homogeneous source term contributions

We first look at the source function contributions $H^\pm(x,\mu)$ from the homogeneous solutions. We apply the chain rule to (B.1), noting that $\mathscr{L}_q[L_{p\alpha}]$ and $\mathscr{L}_q[M_{p\alpha}]$ are known from the linearization analysis of the boundary value problem. All other quantities in (B.1) have vanishing derivatives for

$p \neq q$, so we will drop the index q in the rest of this section. From (B.2) and (B.3), we find

$$\mathscr{L}[X_\alpha^{(P)}(\mu)] = \frac{\omega}{2} \sum_{l=m}^{2N-1} \beta_l P_m^l(\mu) \sum_{j=1}^{N} P_m^l(-\mu_j) w_j \{\mathscr{L}[X_{j\alpha}^{(P)}] + u X_{j\alpha}^{(P)}\}, \tag{C.1}$$

$$\mathscr{L}[X_\alpha^{(N)}(\mu)] = \frac{\omega}{2} \sum_{l=m}^{2N-1} \beta_l P_m^l(\mu) \sum_{j=1}^{N} P_m^l(+\mu_j) w_j \{\mathscr{L}[X_{j\alpha}^{(N)}] + u X_{j\alpha}^{(N)}\}, \tag{C.2}$$

where the layer index q is assumed throughout. The terms with $u\mathbf{X}_\alpha$ arise from the linearization $\mathscr{L}[\omega] = u\omega$.

Next we look at the linearizations of the homogeneous multipliers defined in (B.4) and (B.5). We proceed by chain rule differentiation, using the known result for $\mathscr{L}[k_\alpha]$ from Section 4.2 and the linearization rules $\mathscr{L}[\Delta] = v\Delta$ and $\mathscr{L}[x] = vx$ from Section 4.1. The result for $\mathscr{H}^{++}$ is:

$$\mathscr{L}[\mathscr{H}_\alpha^{++}(x,\mu)] = \frac{-\mathscr{H}_\alpha^{++}(x,\mu)\mu f_\alpha - \mathrm{e}^{-xk_\alpha} x\gamma_\alpha + \mathrm{e}^{-\Delta k_\alpha}\mathrm{e}^{-(\Delta - x)/\mu}[\Delta\gamma_\alpha + (\Delta - x)v\mu^{-1}]}{1 + \mu k_\alpha}, \tag{C.3}$$

where $f_\alpha = \mathscr{L}[k_\alpha]$, and $\gamma_\alpha = vk_\alpha + f_\alpha$. In a similar vein, we find:

$$\mathscr{L}[\mathscr{H}_\alpha^{+-}(x,\mu)] = \frac{\mathscr{H}_\alpha^{+-}(x,\mu)\mu f_\alpha - \mathrm{e}^{-(\Delta - x)k_\alpha}(\Delta - x)\gamma_\alpha + \mathrm{e}^{-(\Delta - x)/\mu}(\Delta - x)v\mu^{-1}}{1 - \mu k_\alpha}, \tag{C.4}$$

$$\mathscr{L}[\mathscr{H}_\alpha^{-+}(x,\mu)] = \frac{\mathscr{H}_\alpha^{-+}(x,\mu)\mu f_\alpha - \mathrm{e}^{-xk_\alpha} x\gamma_\alpha + \mathrm{e}^{-x/\mu}(\Delta - x)v\mu^{-1}}{1 - \mu k_\alpha}, \tag{C.5}$$

$$\mathscr{L}[\mathscr{H}_\alpha^{--}(x,\mu)] = \frac{-\mathscr{H}_\alpha^{--}(x,\mu)\mu f_\alpha - \mathrm{e}^{-xk_\alpha}(\Delta - x)\gamma_\alpha + \mathrm{e}^{-\Delta k_\alpha}\mathrm{e}^{-x/\mu}[\Delta\gamma_\alpha + xv\mu^{-1}]}{1 + \mu k_\alpha}. \tag{C.6}$$

As with the original multipliers, values of these linearizations at the layer boundaries can be obtained by setting $x = 0$ in (C.3) and (C.4), and $x = \Delta$ in (C.5) and (C.6). The above results appeared in SKC in a slightly different form.

C.2. Linearization of the single scatter source term contributions

We start with the definition of $E_p^\pm(x,\mu)$ in (B.10), this time keeping an explicit layer indexing throughout. Applying the linearization operator $\mathscr{L}_q$ for a parameter ξ_q varying in layer q, we find

$$\mathscr{L}_q[E_p^\pm(x,\mu)] = Q_p^\pm(\mu)\{\delta_{pq} u_q \mathscr{E}_p^\pm(x,\mu) + \mathscr{L}_q[\mathscr{E}_p^\pm(x,\mu)]\}. \tag{C.7}$$

$Q_p^\pm(\mu)$ as defined in (B.11) is directly proportional to ω_p, so the corresponding linearization is then $\delta_{pq} u_q Q_p^\pm(\mu)$. For the second term in (C.7), we apply linearization to the definitions of these multipliers given in (B.12). Using the linearizations established in Section 4.1 for $\mathscr{L}_q[\hat{T}_p]$ and

$\mathscr{L}_q[\lambda_p]$, we get

$$\mathscr{L}_q[\mathscr{E}_p^+] = \frac{-\mathrm{e}^{-x\lambda_p}x\chi_{pq} + \mathrm{e}^{-\Delta_q\lambda_p}\mathrm{e}^{-(\Delta_q-x)/\mu}[\Delta_q\chi_{pq} + (\Delta-x)\delta_{pq}v_q\mu^{-1}]}{1+\mu\lambda_p} + \mathscr{E}_p^+\varpi_{pq}^+, \tag{C.8a}$$

$$\mathscr{L}_q[\mathscr{E}_p^-] = \frac{-\mathrm{e}^{-x\lambda_p}x\chi_{pq} + \mathrm{e}^{-x/\mu}[\Delta_q\chi_{pq} + x\delta_{pq}v_q\mu^{-1}]}{1-\mu\lambda_p} + \mathscr{E}_p^-\varpi_{pq}^-, \tag{C.8b}$$

where the dependence of $\mathscr{E}_p^\pm$ on (x,μ) has been assumed, and

$$\varpi_{pq}^\pm = \frac{\mathscr{L}_q[\hat{T}_p]}{\hat{T}_p} \mp \frac{\mu\mathscr{L}_q[\lambda_p]}{1\pm\mu\lambda_p} \quad \text{and} \quad \chi_{pq} = \mathscr{L}_q[\lambda_p] + \delta_{pq}v_q. \tag{C.9}$$

A form of these results were derived for the plane-parallel case in SKC using a perturbation analysis. The above results are a generalization to the average secant pseudo-spherical approximation, and it is clear that there are important contributions to multipliers in layer p from variational derivatives in layer q above p. This illustrates the care that need to be taken in setting up the linearization rules for the pseudo-spherical case.

C.3. Linearization of the classical particular solution source term contributions

From the definition (B.19), we find

$$\mathscr{L}_q[D_p^\pm(x,\mu)] = \mathscr{L}_q[F_p^\pm(\mu)]\mathscr{D}_p^\pm(x,\mu) + F_p^\pm(\mu)\mathscr{L}_q[\mathscr{D}_p^\pm(x,\mu)]. \tag{C.10}$$

For the first term, we note that

$$\mathscr{L}_q[F_p^\pm(\mu)] = \frac{\omega_p}{2}\sum_{l=m}^{2N-1}\beta_l P_m^l(\mu)\sum_{j=1}^{N}P_m^l(-\mu_j)w_j\{\mathscr{L}_q[F_{jp}^\pm] + \delta_{pq}u_qF_{jp}^\pm\}. \tag{C.11}$$

This is similar to the result in (C.1), and follows from the definition in (B.20). Note that the particular solution discrete ordinate vector $\mathbf{F}_p^\pm$ has cross-layer derivatives outside layer p; the linearization of this vector was dealt with in Section 4.3. Finally, since the multipliers $\mathscr{D}_p^\pm$ are actually equal to $\mathscr{E}_p^\pm$, then we may use the results already established for $\mathscr{L}_q[\mathscr{E}_p^\pm]$ in (C.8a) and (C.8b).

C.4. Linearization of the Green's function particular integral source term contributions

Although the Green's function particular integral source term contributions defined in (B.22) have a number of contributions, we may use the results established in Appendices B and C to simplify the analysis considerably. We retain layer indices throughout. In applying chain-rule differentiation to the terms in (B.22), we note that

$$\begin{aligned}&\mathscr{L}_q[a_{p\alpha}X_{p\alpha}^{(P)}(\mu)\mathscr{D}_{p\alpha}^{\pm+}(x,\mu)]\\ &\quad= \delta_{pq}\mathscr{L}_q[a_{p\alpha}X_{p\alpha}^{(P)}(\mu)]\mathscr{D}_{p\alpha}^{\pm+}(x,\mu) + a_{p\alpha}X_{p\alpha}^{(P)}(\mu)\mathscr{L}_q[\mathscr{D}_{p\alpha}^{\pm+}(x,\mu)]\end{aligned} \tag{C.12}$$

since the terms $a_{p\alpha}$ and $X_{p\alpha}^{(P)}(\mu)$ have no optical depth dependence. Their linearizations are given, respectively, by (69) in Section 4.4 and (C.1) above. Similar remarks apply to the combination $b_{p\alpha}X_{p\alpha}^{(N)}(\mu)$ which comprises the second half of (B.22). We are thus left with the task of determining linearizations for the multipliers $\mathscr{D}_{p\alpha}^{\pm\pm}$.

We note that the Green's function multipliers defined in (B.24a) and (B.24b) are expressed in terms of multipliers $\mathscr{H}_p^{\pm\pm}$ and $\mathscr{E}_p^{\pm}$. Since we already have linearizations for these quantities, a straightforward application of the chain rule in terms of known linearizations will yield the desired result. Compacting the notation somewhat by dropping the (x,μ) dependence which is assumed throughout, we find

$$\mathscr{L}_q[\mathscr{D}_{p\alpha}^{+\pm}] = \frac{\varphi_p\{\delta_{pq}\mathscr{L}_q\left[\mathscr{H}_{p\alpha}^{+\pm}\right] + \psi_{pq}\mathscr{H}_{p\alpha}^{+\pm}\} \pm \mathscr{L}_q[\mathscr{E}_p^{+}] - \mathscr{D}_{p\alpha}^{+\pm}\varpi_{pq\alpha}}{\lambda \pm k_\alpha}, \tag{C.13}$$

$$\mathscr{L}_q[\mathscr{D}_{p\alpha}^{-\pm}] = \frac{\varphi_p\{\delta_{pq}\mathscr{L}_q[\mathscr{H}_{p\alpha}^{-\pm}] + \psi_{pq}\mathscr{H}_{p\alpha}^{-\pm}\} \pm \mathscr{L}_q[\mathscr{E}_p^{-}] - \mathscr{D}_{p\alpha}^{-\pm}\varpi_{pq\alpha}}{\lambda \pm k_\alpha}, \tag{C.14}$$

where the following auxiliary quantities are evident:

$$\varphi_p = \hat{T}_p \mathrm{e}^{-\Delta_p\lambda_p}, \tag{C.15}$$

$$\psi_{pq} = \frac{\mathscr{L}_q[\varphi_p]}{\varphi_p} = \frac{\mathscr{L}_q[\hat{T}_p]}{\hat{T}_p} - \Delta_p(\delta_{pq}\lambda_p + \mathscr{L}_q[\lambda_p]), \tag{C.16}$$

$$\varpi_{pq\alpha}^{\pm} = \mathscr{L}_q[\lambda_p] \pm \delta_{pq}\mathscr{L}_q[k_{p\alpha}]. \tag{C.17}$$

This completes the linearization of the Green's function particular integral source term contributions.

Appendix D. Delta-M scaling transformations

We restrict the discussion to an atmosphere with one scatterer. For single scattering albedo ω_q, optical thickness Δ_q and phase function moment coefficients β_{lq} in layer q, the delta-M scaling [22] is

$$\bar{\omega}_q = \omega_q\frac{(1-f_q)}{(1-\omega_q f_q)}, \quad \bar{\Delta}_q = \Delta_q(1-\omega_q f_q) \quad \text{with } \bar{\beta}_{lq} = \frac{\beta_{lq} - f_q(2l+1)}{1-f_q}. \tag{D.1}$$

Here, $l = 0,\ldots,2N-1$ and $f_q = \beta_{Mq}/(2M+1)$ is the *truncation factor* in layer q, with $M = 2N$ indicating that all scaled phase function moment coefficients $\bar{\beta}_{lq}$ for $l \geqslant M$ are zero. As far as the pseudo-spherical approximation is concerned, we note that all spherical optical depths κ_{qp} as defined in (32) scale in the same way as Δ_p.

This result is standard in intensity-only radiative transfer models; see [21] for more details. For a model such as LIDORT with additional inputs $\{u_q, v_q\}$ expressing the relative partial derivatives of ω_q and e_q due to some parameter ξ_q varying in layer q, we must also consider the scaling of these inputs. Remembering that $\mathscr{L}_q[\omega_q] = u_q\omega_q$ and $\mathscr{L}_q[\Delta_q] = v_q\Delta_q$, one can simply apply the linearization

operator to the first two results in (D.1) to define scaled values $\{\bar{u}_q, \bar{v}_q\}$. The result is

$$\bar{u}_q = \frac{u_q}{1-\omega_q f_q} \quad \text{and} \quad \bar{v}_q = v_q - \frac{\omega_q f_q u_q}{1-\omega_q f_q}. \tag{D.2}$$

It is straightforward to extend these scaling results to a layer with a number of particulates, bearing in mind the combination forms

$$\omega_q = \sum_s \omega_{qs}, \qquad \omega_q \beta_{lq} = \sum_s \omega_{qs}\beta_{lqs} \quad \text{and} \quad \omega_q \beta_{lq} u_{lq} = \sum_s \beta_{lqs}\omega_{qs} u_{qs} \tag{D.3}$$

which are used in the RTE (see Section 4.1).

References

[1] Marquardt DW. An algorithm for least squares estimation of nonlinear parameters. J Soc Ind Appl Math 1963;2:431–41.
[2] Rodgers CD. Characterization and error analysis of profiles retrieved from remote sounding experiments. J Geophys Res 1990;95:5587.
[3] Engel HW, Hanke M, Neubauer A In: . Regularization of inverse problems. In Mathematics and its applications, Vol. 375. Dordrecht: Kluwer Academic Publishers, 1996.
[4] Spurr RJD, Kurosu TP, Chance KV. A linearized discrete ordinate radiative transfer model for atmospheric remote sensing retrieval. JQSRT 2001;68:689–735.
[5] Chandrasekhar S. Radiative Transfer. New York: Dover Publications Inc., 1960.
[6] Stamnes K, Tsay S-C, Wiscombe W, Jayaweera K. Numerically stable algorithm for discrete ordinate method radiative transfer in multiple scattering and emitting layered media. Appl Opt 1988;27:2502–9.
[7] Rozanov VV, Diebel D, Spurr RJD, Burrows JP. GOMETRAN: a radiative transfer model for the satellite project GOME—the plane parallel version. J Geophys Res 1997;102:16 683–95.
[8] Rozanov V, Kurosu T, Burrows J. Retrieval of atmospheric constituents in the UV/visible: a new quasi-analytical approach for the calculation of weighting functions. JQSRT 1998;60:277–99.
[9] ESA/ESTEC, Noordwijk, The Netherlands. GOME Users Manual, 1998.
[10] Chance K, Burrows JP, Perner D, Schneider W. Satellite measurements of atmospheric ozone profiles, including tropospheric ozone, from UV/visible measurements in the nadir geometry: a potential method to retrieve tropospheric ozone. JQSRT 1997;57:467–76.
[11] Hoogen R, Rozanov V, Burrows J. Ozone profiles from GOME satellite data: algorithm description and first validation. J Geophys Res 1999;104:8263–80.
[12] Munro R, Siddans R, Reburn WJ, Kerridge BJ. Direct measurement of tropospheric ozone distributions from space. Nature 1998;392:168–71.
[13] van der A RJ, van Oss RF, Kelder H. Ozone profile retrieval from GOME data. In: Russell, J.E. editor. Remote sensing of clouds and the atmosphere III. Proceedings of SPIE Vol. 3495, Barcelona, Spain: SPIE, 1998. 221–9.
[14] Burrows JP, Chance K, Crutzen P, van Dop H, Geary J, Johnson T, Harris G, Isaksen I, Moortgat G, Muller C, Perner D, Platt U, Pommereau J-P, Rodhe H, Roeckner E, Schneider W, Simon P, Sundquist H, Vercheval J. SCIAMACHY: a European proposal for atmospheric remote sensing from the ESA polar platform. Max-Planck Institut für Chemie, Mainz, Germany, 1988.
[15] Callies J, Corpaccioli E, Eisinger M, Lefebvre A, Hahne A. Ozone monitoring by GOME-2 on the METOP satellites. In Atmospheric Ozone. Proceedings of the Quadrennial Ozone Symposium, Sapporo, Japan, 2000.
[16] Stammes P, Levelt P, de Vries J, Visser H, Kruizinga B, Smorenburg C, Leppelmeier G, Hilsenrath E. Scientific requirements and optical design of the ozone monitoring instrument on EOS-CHEM. In SPIE Conference on Earth Observing Systems IV, SPIE Vol. 3750. Denver, USA, 1999. p. 221–32.
[17] van Oss R, Spurr RJD. Fast and accurate 4 and 6 stream linearized discrete ordinate radiative transfer models for ozone profile retrieval. JQSRT 2002;75:177–220.

[18] Dahlback A, Stamnes K. A new spherical model for computing the radiation field available for photolysis and heating at twilight. Planet Space Sci 1991;39:671–83.
[19] Caudill TR, Flittner DE, Herman BM, Torres O, McPeters RD. Evaluation of the pseudo-spherical approximation for backscattered ultraviolet radiances and ozone retrieval. J Geophys Res 1997;102:3881–90.
[20] Siewert CE. A concise and accurate solution to Chandrasekhar's basic problem in radiative transfer. JQSRT 2000;64:109–30.
[21] Thomas GE, Stamnes K. Radiative transfer in the atmosphere and ocean, 1st ed. Cambridge: Cambridge University Press, 1999.
[22] Wiscombe WJ. The delta-M method: rapid yet accurate radiative flux calculations for strongly asymmetric phase functions. J Atmos Sci 1977;34:1408–22.
[23] Kylling A, Stamnes K. Efficient yet accurate solution of the linear transport equation in the presence of internal sources: the exponential-linear-in-depth approximation. J Comp Phys 1992;102:265–76.
[24] Stamnes K, Conklin P. A new multi-layer discrete ordinate approach to radiative transfer in vertically inhomogeneous atmospheres. JQSRT 1984;31:273.
[25] Anderson E, Bai Z, Bischof C, Demmel J, Dongarra J, Du Croz J, Greenbaum A, Hammarling S, McKenney A, Ostrouchov S, Sorensen D. LAPACK User's Guide, 2nd ed. Philadelphia: Society for Industrial and Applied Mathematics, 1995.
[26] Barichello LB, Garcia RDM, Siewert CE. Particular solutions for the discrete-ordinates method. JQSRT 2000;64: 219–26.
[27] McClatchey R, Fenn RW, Selby JE, Volz FE, Garing JS. Environment Research Paper 411, 3rd ed. In Optical properties of the atmosphere. Bedford, MA: Air Force Cambridge, 1972.
[28] Bass AM, Paur RJ. The UV cross-sections of ozone: 1. Measurements in atmospheric ozone. In Proceedings of the Quadrennial Ozone Symposium. Halkidiki, Greece, 1985. p. 606–16.
[29] Chance K, Spurr RJD. Ring effect studies: Rayleigh scattering, including molecular parameters for rotational Raman scattering, and the Fraunhofer spectrum. Appl Opt 1997;36:5224–30.
[30] Bates DR. Rayleigh scattering by air. Planet Space Sci 1984;32:785–90.
[31] Shettle EP, Fenn RW. Models of the aerosols of the lower atmosphere and the effects of humidity variations on their optical properties. Technical Report AFGL-TR-79-0214, Geophysics Laboratory, Hanscomb AFB, MA 01732, 1979.
[32] Bhartia PK, McPeters RD, Mateer CL, Flynn LE, Wellemeyer C. Algorithm for the estimation of vertical ozone profiles from the backscattered ultraviolet technique. J Geophys Res 1996;101:18 793–806.
[33] Rozanov AV, Rozanov VV, Burrows JP. Combined differential-integral approach for the radiation field computation in a spherical shell atmosphere: Nonlimb geometry. J Geophys Res 2000;105:22 937–42.
[34] Stam D, de Haan JF, Hovenier JW, Aben I. Detecting radiances in the O_2 A band using polarization sensitive satellite instruments, with application to GOME. J Geophys Res 2000;105:22 379–92.
[35] Lacis AA, Chowdhary J, Mischenko MI, Cairns B. Modelling errors in diffuse-sky radiation: vector vs. scalar treatment. Geophys Res Lett 1998;25:135–8.
[36] Mischenko MI, Travis LD. Satellite retrieval of aerosol properties over the ocean using polarization as well as intensity of reflected sunlight. J Geophys Res 1997;102:16 989–7013.
[37] Deuzé JL, Bréon FM, Deschamps PY, Devaux C, Herman M, Podaire A, Roujean JL. Analysis of the POLDER (Polarization and Directionality of Earth's Reflectances) airborne instrument observations over land surfaces. Remote Sensing Environ 1993;45:137–54.
[38] Schulz FM, Stamnes K. Angular distribution of the Stokes vector in a plane-parallel vertically inhomogeneous medium in the vector discrete ordinate radiative transfer (VDISORT) model. JQSRT 2000;65:609–20.
[39] Siewert CE. A discrete-ordinates solution for radiative-transfer models that include polarization effects. JQSRT 2000;64:227–54.